Ecological Monographs, 71(4), 2001, pp. 557–586

A METHOD FOR SCALING VEGETATION DYNAMICS: THE ECOSYSTEM DEMOGRAPHY MODEL (ED)

P. R. MOORCROFT,[1,3] G. C. HURTT,[2] AND S. W. PACALA[1]

[1]*Department of Ecology and Evolutionary Biology, Princeton University, Princeton, New Jersey 08544-1003 USA*
[2]*Complex Systems Research Center, Institute for the Study of Earth, Oceans, and Space, University of New Hampshire, Durham, New Hampshire 03824 USA*

Abstract. The problem of scale has been a critical impediment to incorporating important fine-scale processes into global ecosystem models. Our knowledge of fine-scale physiological and ecological processes comes from a variety of measurements, ranging from forest plot inventories to remote sensing, made at spatial resolutions considerably smaller than the large scale at which global ecosystem models are defined. In this paper, we describe a new individual-based, terrestrial biosphere model, which we label the ecosystem demography model (ED). We then introduce a general method for scaling stochastic individual-based models of ecosystem dynamics (gap models) such as ED to large scales. The method accounts for the fine-scale spatial heterogeneity within an ecosystem caused by stochastic disturbance events, operating at scales down to individual canopy-tree-sized gaps. By conditioning appropriately on the occurrence of these events, we derive a size- and age-structured (SAS) approximation for the first moment of the stochastic ecosystem model. With this approximation, it is possible to make predictions about the large scales of interest from a description of the fine-scale physiological and population-dynamic processes without simulating the fate of every plant individually. We use the SAS approximation to implement our individual-based biosphere model over South America from 15° N to 15° S, showing that the SAS equations are accurate across a range of environmental conditions and resulting ecosystem types. We then compare the predictions of the biosphere model to regional data and to intensive data at specific sites. Analysis of the model at these sites illustrates the importance of fine-scale heterogeneity in governing large-scale ecosystem function, showing how population and community-level processes influence ecosystem composition and structure, patterns of aboveground carbon accumulation, and net ecosystem production.

Key words: biogeochemical dynamics; ecosystem dynamics; ecosystem model, terrestrial; individual-based model; moment approximation; plant community dynamics; scaling; size- and age-structured; South America; sub-grid scale heterogeneity; terrestrial biosphere model; vegetation dynamics.

INTRODUCTION

The past decade has seen remarkable progress in the development of global ecosystem models capable of reproducing a number of important features of the Earth's vegetation. Land surface models such as SiB (Sellers et al. 1986, 1997), LSX (Pollard and Thompson 1995), LSM (Bonan 1995), and BATS (Dickinson et al. 1993) now routinely predict diurnal and seasonal CO_2 and moisture fluxes; biogeochemistry models such as TEM (Reich et al. 1991, Melillo et al. 1993), CASA (Potter et al. 1993), and Century (Parton et al. 1993) predict global nutrient dynamics; biogeographic models such as BIOME (Prentice et al. 1992, Haxeltine et al. 1996, Haxeltine and Prentice 1996) predict the distribution of vegetation types; and a new class of models led by IBIS (Foley et al. 1996) does all of these while interacting with a general circulation model (GCM). However, efforts to develop the next generation of models capable of predicting the transient responses of global ecosystems to land use and climate change are fundamentally hampered by the existence of important fine-scale heterogeneity within ecosystems.

Ecologists distinguish two qualitatively different sources of ecosystem heterogeneity. Exogenous or abiotic heterogeneity arises from variation differences in the physical environment such as variation in topography, climate, and soil parent material. Endogenous or biotic heterogeneity arises spontaneously even in a physically homogeneous environment. Two of the most important natural processes causing biotic heterogeneity within ecosystems are the mortality of large adult trees and disturbances such as fire or windthrow. These stochastic events give rise to significant spatial heterogeneity in resource availability, altering the subsequent dynamics of the local plant canopy and belowground ecosystem.

We now offer two examples that illustrate the importance of endogenous heterogeneity for ecosystem processes that motivate the modeling approach offered

Manuscript received 5 August 1999; revised 20 April 2000; accepted 3 May 2000; final version received 13 April 2001.

[3] Present address: Department of Organismal and Evolutionary Biology, Harvard University, Cambridge, Massachusetts 02138 USA. E-mail: prmoorcroft@oeb.harvard.edu

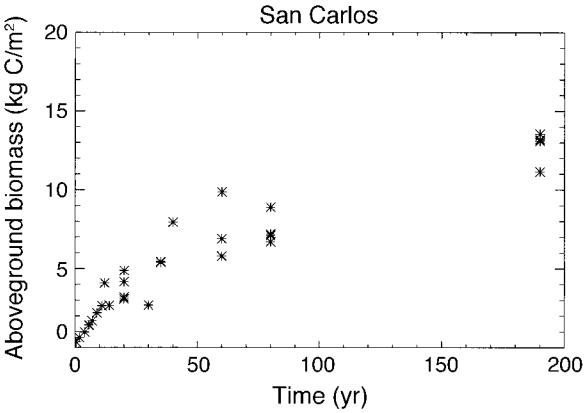

FIG. 1. Chronosequence of aboveground biomass (kg C/m^2) at San Carlos, Venezuela (2° N, 68° W), a tropical forest site, recorded by Uhl (1987) and Saldarriaga et al. (1988).

in this paper. The first concerns the rate at which abandoned agricultural land in the tropics takes up atmospheric carbon, an issue central to planning mitigation strategies to combat rising atmospheric CO_2. Fig. 1 shows the accumulation of aboveground carbon at San Carlos, a moist tropical forest in Venezuela (Saldarriaga et al. 1988) as a function of successional age (time since abandonment of slash-and-burn agriculture). The greater than 200-yr timescale of uptake is surprisingly long, especially because net primary productivity (NPP) is high throughout the chronosequence shown, 1.1–1.2 kg $C \cdot m^{-2} \cdot yr^{-1}$ (Uhl 1987), thus ruling out the time required to rebuild depleted soil fertility as an explanation for the length of the timescale. With more than half of a tree's NPP going to wood production (Uhl and Jordan 1984, Saldarriaga et al. 1988), one would expect that the time required to accumulate 12 kg C/m^2 above ground would be an order of magnitude shorter than is observed. Indeed, most global ecosystem models would predict a short timescale for this process (Reich et al. 1991, Potter et al. 1993, Foley et al. 1996).

The detailed surveys of the plots at San Carlos provide an explanation for the long timescale of carbon uptake (Uhl 1987, Saldarriaga et al. 1988). As we show, the rate of carbon accumulation at San Carlos is explained by height-structured competition, the presence of successional diversity, and the demography of size and age distributions. Because of the difficulty of phenomenologically parameterizing the outcome of size- and age-structured competition between plants of different types under different environmental conditions, size- and age-structured ecosystem models may be necessary to predict transient carbon dynamics and fluxes.

The second example concerns the inference drawn from measurements of carbon uptake by forests, like those sought by the FLUXNET network of eddy-correlation towers (Baldocchi et al. 1996, Baldocchi and Falge 1998). Consider an old-growth forested landscape with zero net carbon uptake (zero net ecosystem production or NEP). Such landscapes are inevitably fine-grained mosaics at canopy tree scales. Some places have high carbon loss rates because a large tree has recently died in them and is decomposing, while the majority take up carbon because they contain a growing tree and their former occupant has largely finished decomposing. Thus, the distribution of local NEP in this example has zero mean but high variance. An understanding of this large variance is critical to interpreting NEP measurements like those obtained from eddy-flux towers (Phillips et al. 1998). If the length scale of the tower's footprint is large relative to the spatial scale of disturbance (which correlates with the scale of canopy tree deaths), then the tower will measure the correct landscape average NEP. In contrast, if the length scale of disturbance is sufficiently large, then the tower is unlikely to report the landscape average NEP. The important point here is that the interpretation of flux measurements requires an understanding of the size, age, and fine-scale spatial structure of local patches in the landscape.

The concerns raised by these examples are not new. Ecosystem modelers have addressed the issue of endogenous heterogeneity for nearly three decades using forest gap models (Botkin et al. 1972*a*, Shugart and West 1977, Huston et al. 1988, Smith and Urban 1988, Urban 1990, Huston 1992, Pacala et al. 1996). A gap model is a stochastic process that predicts the fate of every individual inhabiting an area the size of a canopy tree. This area is labeled a ''gap.'' Individuals in the gap compete for light, water, and nutrients. The model is stochastic because of the stochastic nature of birth, death, and dispersal. To make predictions at scales of a forest stand or larger, runs for an ensemble of coupled or uncoupled gaps are summed or, equivalently, averaged.

The widespread success of gap models is derived in large part from the small scale of their formulation (Huston et al. 1988). These models naturally capture the gap-scale heterogeneity created by the deaths of single canopy trees, and the height-structured competition among saplings competing to fill an opening in the canopy. As we show, they are thus able to reproduce the kinds of phenomena illustrated in the two examples above. Moreover, because the models are formulated at the scales at which field biologists work, it is comparatively straightforward to measure relevant parameters (Pacala et al. 1996) and compare to data on forest structure (Huston 1992). Modern gap models that demonstrably reproduce the transient details of succession are routinely used to manage forested ecosystems (e.g., Lindner 1999). They have also been extended to other terrestrial ecosystems, including shrublands and grasslands (Coffin and Lauenroth 1990), and are commonly used to investigate the consequences of global change (Solomon 1986, Smith et al. 1992, Bolker et al. 1995, Shugart and Smith 1996).

Even so, the fact that a 1° GCM grid cell would contain between 10^8 and 10^9 modeled gaps has largely prevented the development of global gap models. One exception is the Hybrid model of Friend et al. (1997). The Hybrid model replaces the species-specific functions in most gap models, with the general physiological and biogeochemical relationships in large-scale ecosystem models such as IBIS, Century, and BIOME. It thus combines the generality of the large-scale ecosystem models with the mechanistic rigor and facility of measurement that characterize the small-scale gap models. It attempts to overcome the scale mismatch by calculating, for each GCM grid cell, the ensemble average of 10 stochastic runs of a single, canopy-sized gap. Although this may be sufficient under the most favorable of circumstances, our work indicates that most circumstances will require much larger ensembles of hundreds or thousands of gap-scale realizations for each GCM grid cell because of biodiversity and the heterogeneity caused by natural and human disturbances.

What is needed to scale from gap to global dynamics is a way to derive the equations governing the ensemble average of a stochastic gap model directly from the fine-scale processes in it. This scaling would be analogous to the statistical physics used to derive the Navier-Stokes equations in a GCM from the stochastic process of molecular motion (rather than the classical derivation from fluid flow). In this paper, we introduce a physiologically based stochastic gap model, similar to Hybrid, and then derive a set of partial differential equations that govern its ensemble average. These equations scale the processes in the gap model and represent an ecological ''statistical mechanics.'' Their advantages are first, that computer time is greatly reduced from that required by brute-force simulation, and second, that their mathematical compactness provides opportunity for direct mathematical analysis, at least in some cases. We suspect that our method of scaling will work generally for individual-based simulators of vegetation dynamics. A preliminary report on the method is found in Hurtt et al. (1998).

After deriving the equations for the ensemble average, and showing that they work for our physiological gap model, we implement the model on a $1° \times 1°$ grid for tropical and subtropical South America between 15° N to 15° S. It is important to understand that the model includes no abiotic heterogeneity within the 1° grid cells, caused for example by sub-grid scale variation in topography and soil parent material. The model does include biotic heterogeneity within each grid cell and abiotic heterogeneity in climate and soil characteristics between grid cells.

We then evaluate the regional predictions of the model by comparing them to corresponding estimates of NPP, aboveground biomass, and soil carbon. Evaluating the model at this scale is difficult however, due to the incompleteness of regional data sets and absence of model intercomparisons such as the VEMAP exercise for North American continent (VEMAP Members 1995, Kittel et al. 1997). To supplement the broadscale comparisons, we investigate the predicted ecosystem composition and structure at three locations in detail. These examples illustrate ways in which the fine-scale mechanisms in gap models create endogenous sub-grid scale heterogeneity that leads to large-scale pattern that is captured using the SAS approximation.

Model

The ecosystem demography model (ED) predicts above- and belowground ecosystem structure and the fluxes of carbon and water between the ecosystem and the atmosphere from climate and soil properties. It links together phenomena operating at a range of temporal scales from the fast-scale responses of plant physiology to changes in weather (hourly), through medium-scale changes in soil hydrology and phenology (weekly, seasonal), and slow-scale changes in the composition of vegetation and belowground carbon stores (yearly, decadal, century). It consists of an individual-based vegetation model describing the growth, reproduction, and mortality dynamics of a plant community coupled to biogeochemical models describing the associated belowground fluxes of carbon, water, and nitrogen. In the paper, we implement the model first as a stochastic, individual-based, gap simulator similar to the Hybrid model developed by Friend et al. (1997) and then as a size- and age-structured (SAS) approximation. The state variables of the stochastic simulator are the sizes, locations, and functional types of individual plants and the belowground nitrogen, water, and carbon in each canopy-tree-sized spatial cell (15×15 m). In the SAS approximation, the equations of the individual-based gap simulator become terms within systems of partial differential equations (PDEs). These size- and age-structured equations closely approximate the first moment of the stochastic processes in the gap simulator. Thus, the state variables in the SAS approximation predict the mean characteristics of the ecosystem at the scale of the grid cell by correctly averaging the fine-scale processes in the individual-based gap simulator.

The components of ED draw heavily on established sub-models formulated by others over the past three decades. In particular, the structure of our stochastic gap model incorporates many of the developments in individual-based ecosystem modeling, including explicit representation of competition for water (Shugart and West 1977, Mann and Post 1980, Shugart 1984, Pastor and Post 1985, Bonan 1989), carbon and nitrogen dynamics above- and belowground (Aber et al. 1982, Pastor and Post 1985, Post and Pastor 1996), the use of plant functional types (Noble and Slatyer 1980, Huston and Smith 1987, Smith and Huston 1989), and a leaf-level formulation for photosynthesis and evapotranspiration (Friend et al. 1997). This paper represents our first attempt to bring these elements together. To

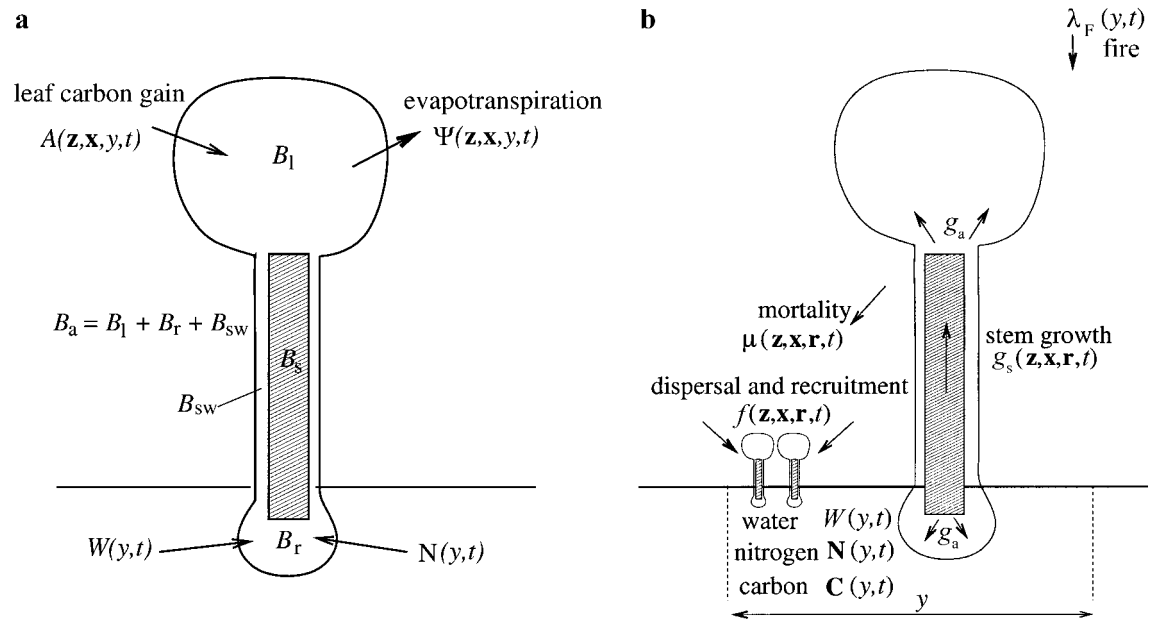

FIG. 2. (a) Individual-level fluxes of carbon, water, and nitrogen and the partitioning of carbon between active and structural tissues (B_a and B_s, respectively). (b) Summary of the processes occuring within each gap y. Each plant's structural and living tissues grow at rates g_s and g_a, respectively. Individuals die stochastically at rate μ and give birth to offspring at rate f, which are then dispersed randomly across gaps. These vital rates vary as a function of the type (**x**), size (**z**) and resource environment (**r**) of the plant. Fires occur stochastically at rate λ_F calculated by the fire sub-model. Hydrologic and decomposition sub-models track the dynamics of water (W), carbon (C), and nitrogen (N) within each gap.

facilitate the incorporation of future improvements, we have designed the model with a modular structure that permits alternative sub-models to be swapped for those currently implemented.

In the current version, climate and soil properties within each 1° grid cell are specified from the ISLSCP (International Satellite Land Surface Climatology Project) Initiative I global data set (Meeson et al. 1995, Sellers et al. 1995). The ISLSCP data set was specifically designed for large-scale biosphere modeling, providing a consistent global data set of climatological variables and soil characteristics. A preliminary review suggested that the data set is comparable in quality to other global data sets (Kerr 1995); however, subsequent analyses have identified several shortcomings. In particular, while the data set provides global coverage, its temporal coverage is short, containing only two representative years of climate data. With regard to the South American continent, the quality of the precipitation data is reduced because of sparse gauge coverage (Kerr 1995), and the estimate of downward shortwave radiation over the Amazon basin is thought to contain a significant degree of error (Morrill 1999). Although the implementation described here relies on ISLSCP data, the model can be driven from other sources of data including output from a climate model.

Overview of stochastic gap model

The individual plants in the model have the structure shown in Fig. 2a. Each plant has living tissue, with biomass B_a distributed among leaves (B_l), sapwood (B_{sw}) and roots (B_r), and a dead structural stem, with biomass B_s (see Table 1 for a list of model parameters). A mechanistic sub-model describes net carbon uptake (A_n) and water loss (Ψ) by a plant's leaves on an hourly timescale, as a function of light availability, temperature, and humidity. Soil water (W) and mineralized nitrogen (N) are taken up by the roots to meet demand, and limit A_n and Ψ when sufficiently depleted. The dynamics of soil water, nitrogen, and organic carbon are governed by a simple one-layer hydrology model and a modification of the Century model (Parton et al. 1987, 1993).

As plants gain carbon and nitrogen, they grow and allocate the new tissue to roots, live and dead stem, leaves, and reproduction according to empirical allometric relationships. Individuals die stochastically by windthrow and other forms of density-independent mortality with the probability of mortality varying between the different plant types. Individuals also die at elevated rates if they are in unfavorable carbon balance (Fig. 2b).

The individual plants occur in a series of discrete spatial areas called gaps, each approximately the size of a single canopy tree's crown area (15 × 15 m). The gaps within each 1° × 1° GCM grid cell (~12 000 km^2 at the equator), indexed by the symbol y, are coupled only by exchanging seeds, by sharing the same fire regime, and by sharing the same climatology and soil characteristics specified from the 1° ISLSCP data set

TABLE 1. Ecosystem demography model parameters.

Parameter	Quantity	Units
Aboveground state variables		
$n(\mathbf{z}, \mathbf{x}, a, t)$	density† of size $\mathbf{z}$ type $\mathbf{x}$ plants in gaps of age a at time t	m^{-2}
$p(a, t)$	distribution of gap ages a at time t	dimensionless
State dimensions		
$\mathbf{z}$	plant size $\mathbf{z} = [z_s, z_a] = [B_s, B_a]$	kg C, kg C
$\mathbf{x}$	plant type $[x_1, x_2] \cdot x_1 = 0$ if C_3, 1 if C_4, x_2 = leaf longevity	dimensionless, yr
a	gap age	yr
t	time	yr
Plant resource environment		
$\mathbf{r}$	resource vector $\mathbf{r} = [\phi, W, N]$	$J \cdot m^{-2} \cdot s^{-1}$, m^3 H_2O/m^2, kg N/m^2
ϕ	photosynthetically active radiation (PAR)	$J \cdot m^{-2} \cdot s^{-1}$
W	soil water content	m^3 H_2O/m^2
N	plant available soil nitrogen content	kg N/m^2
Transition rates		
g_s	structural biomass growth rate	kg C/yr
g_a	living biomass tissue growth rate	kg C/yr
μ	mortality rate	yr^{-1}
f	fecundity	yr^{-1}
λ	total disturbance rate $\lambda = \lambda_F + \lambda_{DI}$	yr^{-1}
λ_F	fire frequency	yr^{-1}
λ_{DI}	rate of canopy gap formation	yr^{-1}
s	survivorship of plants following disturbance	dimensionless
Plant size characteristics		
h	height	m
B_a	living biomass ($B_l + B_r + B_{sw}$)	kg C
B_s	structural stem biomass	kg C
B_l	leaf biomass	kg C
B_r	root biomass	kg C
B_{sw}	sapwood biomass	kg C
Leaf-level carbon and water fluxes		
A_n	net rate of carbon gain per unit leaf area	$\mu mol\ C \cdot m^{-2} \cdot s^{-1}$
Ψ	evapotranspiration rate per unit leaf area	$\mu mol\ H_2O \cdot m^{-2} \cdot yr^{-1}$
Decomposition model state variables and coefficients		
C_1	fast soil carbon pool	kg C/m^2
C_2	structural soil carbon pool	kg C/m^2
N_1	fast soil nitrogen pool	kg N/m^2
N_2	structural soil nitrogen pool	kg N/m^2
Miscellaneous		
$n_0(\mathbf{z}, \mathbf{x}, a)$	initial plant density $n(\mathbf{z}, \mathbf{x}, a, 0)$†	m^{-2}
$p_0(a)$	initial gap age distribution	dimensionless
$\mathbf{z}_0$	seedling size	kg C, kg C
y	integer gap number $(1. . .Q)$	dimensionless
h^*	height above which mortality is treated as disturbance	m
c_s	stomatal conductance	$\mu mol\ H_2O \cdot m^{-2} \cdot s^{-1}$
T_L	leaf temperature	°C
T_A	atmospheric air temperature	°C
C_i	interstitial concentration of CO_2	mol/mol
C_a	atmospheric concentration of CO_2	mol/mol

† $n(\mathbf{z}, \mathbf{x}, a, t)$ is technically a density distribution where $n(\mathbf{z}, \mathbf{x}, a, t)dz_s dz_a da$ is the per m^{-2} density of type $\mathbf{x}$ plants between size z_s and $z_s + dz_s$, and size z_a and $z_a + dz_a$ in gaps aged between a and $a + da$ at time t.

(Fig. 2b). There is no exchange of water or nitrogen among gaps, nor any cross-gap shading, nor any communication between gaps in adjoining GCM grid cells. Each plant within a gap has a size $\mathbf{z}$, but horizontal positions are not specified. Thus, the simulator has spatial geometry similar to the FORET and FORCLIM gap models (Shugart and West 1977, Shugart 1984, Bugmann 1996).

Before proceeding further, readers should be aware of the following minor departures from conventional notation. Each plant is composed of B_s, B_l, B_r, and B_{sw} (Fig. 2) and has a height and diameter; however, the allometry described below allows us to compute all of these properties from the biomass of the structural stem B_s and active tissues B_a alone. Thus the size vector $\mathbf{z}$ is two dimensional and equals $[B_s, B_a]$. In Fig. 2 and throughout, size $\mathbf{z}$ and time t are true continuous variables as written, but the gap label y is discrete. Finally, the functional type designation $\mathbf{x}$ contains a mix of a discrete category (C_3 vs. C_4) and a continuous trait variation (leaf longevity). We now describe each component of the gap model; the detailed structure of the component sub-models is provided in a series of Appendices A–I.

Leaf physiology

The fast timescale engine of our model is a sub-model for carbon uptake and evapotranspiration for each plant. Our formulation is taken almost entirely from IBIS (Foley et al. 1996), and is based on the schemes developed by Farquhar, Collatz, Ball, Berry, and others (Farquhar and Sharkey 1982, Ball et al. 1986, Collatz et al. 1991, 1992), for predicting potential carbon fixation and evapotranspiration per unit leaf area from standard climatological inputs. Similar formulations are found in other ecophysiological models (Foley et al. 1996, Haxeltine and Prentice 1996, Friend et al. 1997, Sellers et al. 1997). Our sub-model contains no novel formulations of these underlying physiological processes.

The sub-model calculates the hourly dynamics of carbon uptake and evapotranspiration by solving the following system of five equations (specified in full in Appendix A):

1) An equation for the net rate of carbon gain per unit leaf area (A_n), as a function of leaf temperature (T_L), absorbed photosynthetically active radiation (PAR), and C_i, the interstitial concentration of CO_2. This is the familiar model of the light and dark reactions of C_3 photosynthesis, tracing to Farquhar (Farquhar and Sharkey 1982) with leaf respiration proportional to the maximum rate of carboxylation. A separate equation governs C_4 photosynthesis (Collatz et al. 1992).

2) An equation for the rate of evaporative water loss (Ψ) per unit leaf area, as a function of stomatal conductance (c_s), T_L(which determines the mole fraction of water vapor in the saturated interstitial air), and the mole fraction of water vapor in the atmosphere.

3) A simple diffusion scheme giving C_i as function of c_s, the concentration of atmospheric CO_2 (C_A), and A_n.

4) An equation for $c_s$as a function of A_n, C_i, and the water vapor gradient between the inside of the leaf and the atmosphere. This is the stomatal conductance model of Leuning (Leuning 1995), which is itself based on that of Ball and Berry (Ball et al. 1986).

5) An energy balance equation giving T_L from the balance of radiation inputs and evaporative and convective cooling.

Collectively, the equations are solved for the five unknowns, A_n, Ψ, T_L, C_i, and c_s, given air temperature, C_A, atmospheric water vapor, and incoming photosynthetically active radiation (PAR). The climatological drivers necessary for solving (1)–(5) could be supplied interactively by a climate model, but in this implementation are specified from the ISLSCP I global climatological data set (Meeson et al. 1995, Sellers et al. 1995). The ISLSCP data set provides three-hourly climatology for an average day in each month on a $1^\circ \times 1^\circ$ degree spatial grid, which we interpolate to provide the hourly climatological data.

The physiological sub-model yields potential evapotranspiration and carbon gain rates of an individual for conditions in which soil nutrients and water are not limiting. We account for the influence of nitrogen and water availability by solving (1)–(5) under the condition of stomatal closure (stomatal conductance set equal to cuticular conductance). Belowground resource limitation causes an individual's A_n and Ψ values to move from their potential toward their shutdown values in a graded manner (Appendix B). Also, if soil-water limitation becomes too severe, then plants drop their leaves, losing a portion of their leaf biomass (Appendix E).

To speed computation, rather than repeatedly solving for the carbon gain and evapotranspiration of each individual at each time step, we calculated hourly solutions of (1)–(5) at 120 light levels between 0% light and 100% PAR (full sun) and integrated these values over each month in each 1° grid cell. We compile these values into a look-up-table of monthly potential and shutdown values of A_n and Ψ for each grid cell at different light levels. The look-up-table allows us to take time steps of days-to-weeks rather than hourly (the actual time step is adaptive), while still accounting for the diurnal cycles of the physiological processes and incoming climatology (PAR, temperature, and humidity) that affect photosynthetic rates. The leaf-level carbon and water fluxes of each individual are calculated from the potential and shutdown values by determining the current extent of stomatal closure (determined by current water and nitrogen availability, see Appendix B) and using this value to interpolate between the potential and shutdown values of carbon and water uptake rate obtained from the look-up-table. The net carbon uptake and evapotranspiration of the individual is then calculated by multiplying its per unit leaf area carbon and water fluxes by its total leaf area and then deducting growth respiration and tissue respiration costs, which are temperature-dependent proportions of its leaf, root, and sapwood biomass (see Appendix E).

Plant functional diversity

Ecosystem models typically represent the vast array of differences in plant structure and function by dividing the earth's vegetation into a few discrete plant functional types (Foley et al. 1996, Haxeltine and Prentice 1996, Friend et al. 1997, Sellers et al. 1997) such as C_4 grasses, shrubs, broadleaf trees, and evergreen conifers. This approach has been successfully applied in several individual-based, stochastic gap models for plant communities with high species-level diversity (Noble and Slatyer 1980, Huston and Smith 1987, Smith and Huston 1989).

Recently, Reich et al. (1997) have provided an empirical framework for specifying the characteristics of plant functional types (Fig. 3). The upper two panels of Fig. 3 show the relationships, across hundreds of species, between leaf life span, specific leaf area, and foliar nitrogen concentration. From left to right along

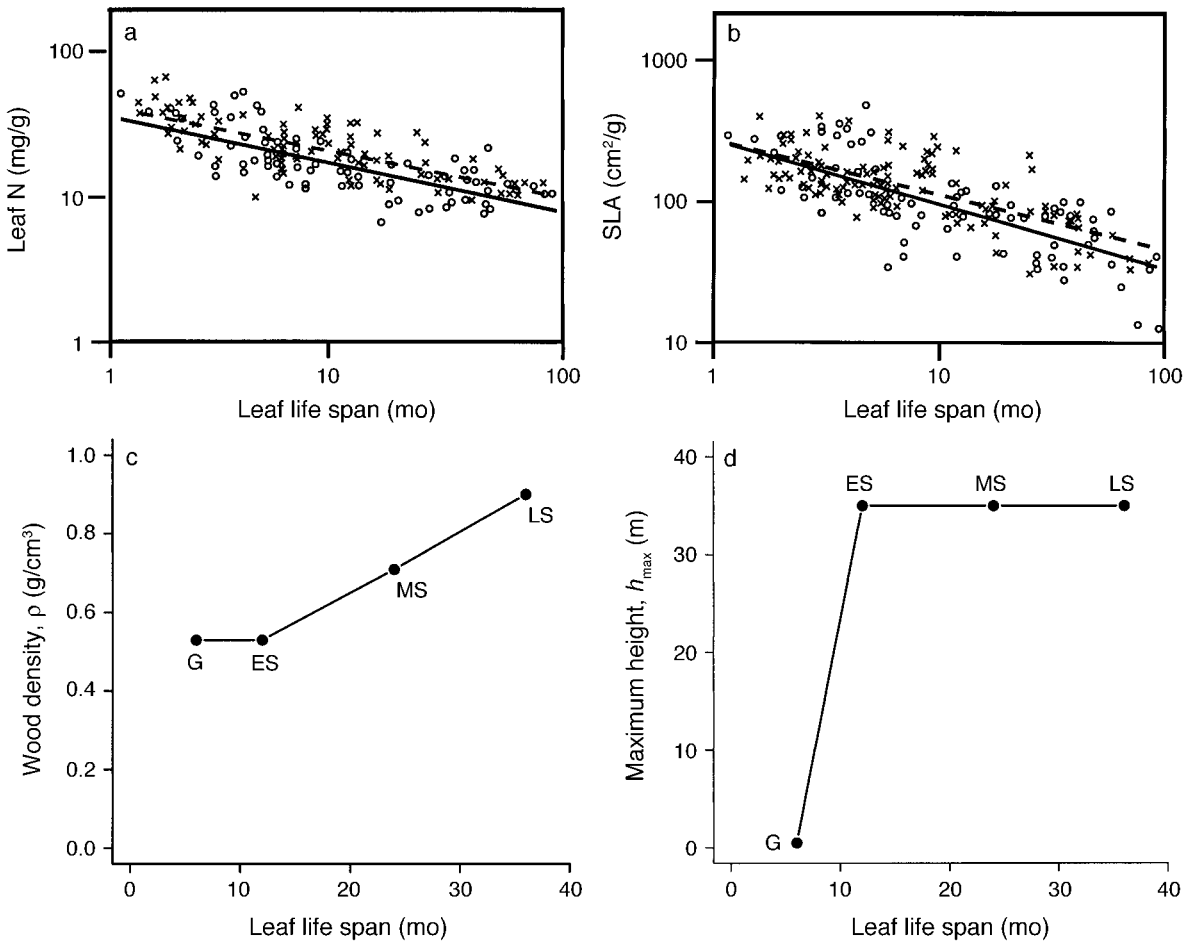

FIG. 3. Continuum of plant traits used to specify the characteristics of the plant functional types. Panels a and b show the correlated changes in leaf physiological characteristics identified by Reich et al. (1997): (a) relationship between leaf nitrogen content and leaf longevity and (b) relationship between specific leaf area (SLA) and leaf longevity (redrawn from Reich et al. [1997]). Panels c and d show the associated variation in plant structural characteristics used to specify the plant-level properties of C_4 grasses (G), and early (ES), mid- (MS), and late (LS) successional tree types: (c) the relationship between wood density and leaf longevity and (d) the relationship between maximum size and leaf longevity.

the axis in each panel, the species change from grasses and forbs to shrubs and pioneer tree species, then to broadleaf deciduous trees, then to broadleaf evergreens, and finally to evergreen conifers (see Reich et al. 1997).

Our representation of functional diversity is built around the relationship shown in the upper panels of Fig. 3, adding to these whether the plant is C_3 or C_4 and two attributes of plant structure, wood density and maximum height (see lower panels of Fig. 3). The position of a functional type on these continuous axes together with its designation as C_3 or C_4 is given by the vector **x**. For the regional model described in this paper, we specified four plant functional types, C_4 grasses and pioneer, mid-, and late successional broadleaf trees (parameter values in Appendix C). The C_4 grass accumulates carbon rapidly due to its high specific leaf area, and its C_4 leaf physiology enables it to maintain this rate at high temperatures. The three types of tree are all C_3 but vary in specific leaf area and wood density. The pioneer type has high specific leaf area and low wood density, enabling rapid carbon accumulation and height growth while the late successional type has a low specific leaf area and high wood density so it accumulates carbon more slowly and has slower height growth. These differences in carbon accumulation and height growth rates between the different tree types are counterbalanced by differences in leaf life span, which influence their ability to persist and grow at low light levels in the forest understory and in their mortality rates, which determine adult longevity (details given in *Model: Mortality*).

Individual allocation, growth, and recruitment

Plants grow by allocating fixed carbon from the model of leaf physiology to various tissues. Because reliable mechanistic models of dynamic plant allocation do not yet exist, we have chosen to take an empirical

approach. We derive our allocation scheme by inverting empirical allometric equations for the patterns of allocation that they imply. The plants in our model thus allocate to stay on data-defined allometries.

For aboveground allometry, we used data on the biomass of various plant components from a tropical forest site in Venezuela in relation to their height, diameter, and wood density (Saldarriaga et al. 1988) and from a survey of the height and diameter of 56 tropical tree and shrub species O'Brien et al. (*unpublished manuscript*). Fine root biomass was calculated assuming that plants allocate to maintain an approximately equal amount of foliar and fine root biomass. Sapwood allocation was calculated using a pipe model, which specifies that sapwood cross-sectional area within the stem is proportional to leaf area (Shinozaki et al. 1964*a*, *b*). Collectively, we use these empirical data and relationships to compute the height and diameter of plants, and the partitioning of their carbon into living (leaves, fine roots, sapwood) and structural components (bole and structural root biomass). Due to their differences in wood density (Fig. 3c) the different tree functional types have different rates of stem growth: for a given rate of investment in structural carbon, pioneers grow rapidly in height while the mid- and late successional trees grow more slowly.

In the model, plants first allocate net incoming carbon (gross photosynthesis minus respiration) to replace lost leaf and fine root tissues. They then allocate what is left to growth and reproduction. The fraction going to reproduction is a constant for all species and is set to a value consistent with seed trap data. Finally, the carbon left for growth is allocated to keep plants on the empirical allometries. If plants are in negative carbon balance, living biomass shrinks due to respiration and decay of active tissues, but this is relatively unimportant because of the high mortality rates of plants in negative carbon balance (see *Model: Mortality*). The differences in leaf longevities identified by Reich et al. 1997 (Fig. 3) cause differences in the tissue loss rates of the different plant functional types. In particular, the higher leaf longevities of the mid- and late successional trees increase their ability to persist and grow at low light levels in the understory. Since the allocation functions are empirical, the allocation of carbon within plants in the model matches that found in the field. Details on allocation and growth can be found in Appendices D and E.

Previous theoretical work has suggested that recruitment limitation can be a significant factor influencing the species-level composition of plant communities (Clark and Ji 1995, Hurtt and Pacala 1995), and at least in some cases, this appears to be borne out empirically (Clark et al. 1998). This sensitivity to recruitment at the species level is thought to be particularly important in species-rich communities because the average number of individuals per species within dispersal range of a given location is low. As a result, the probability that propagules of all species will be found at a given location is small, increasing the likelihood that chance dispersal events will determine local community composition.

For similar reasons, theoretical analyses suggest that recruitment limitation is unlikely to be a significant factor influencing composition at the scale of plant functional types (Pacala and Tilman 1993, Hurtt and Pacala 1995). As one divides biodiversity into progressively fewer types, the average number of individuals per type increases, thereby increasing the probability that propagules of each type will be found at every location, reducing the importance of chance dispersal events. In addition, at the scale of plant functional types, distinctions among competitors become large, making competitive contests between individuals more deterministic.

In this implementation of ED, relatively few functional types are represented and we are not attempting to model range shifts. For these reasons and to reduce model complexity, we have implemented the simplest of dispersal and recruitment models. We assume random dispersal between gaps within the same grid cell. All recruits have the same minimum size ($\mathbf{z}_0$), and the same survivorship to establishment. To calculate the number of recruits in any time interval, we divide the fraction of the total reproductive output that survives to establishment by the carbon required to produce an individual of size $\mathbf{z}_0$, a quantity which is determined from the allometry. The remaining fraction of reproductive output is loaded into the decomposition submodel. Note that it is possible to relax these assumptions. For example, in Hurtt et al. (1998) we presented a formulation with explicit within- and between-gap dispersal rates.

Mortality

The mortality rates of plants in the model are divided into two components. The first reflects differential longevities of the plant functional types. While pioneers have high rates of carbon accumulation and can grow quickly in height, empirical data show they experience higher rates of mortality compared to late successional trees (Putz et al. 1983, Augspurger and Kelly 1984, Lawton 1984). The high mortality of pioneer species is thought to be largely biomechanical: their low wood density makes them susceptible to pathogen attack in the understory (Augspurger and Kelly 1984) and to windthrow disturbance in the tree canopy (Putz et al. 1983, Augspurger and Kelly 1984, Lawton 1984). We included these longevity differences by specifying a negative relationship between wood density and mortality consistent with empirical estimates for tropical trees (Uhl and Jordan 1984, Swaine et al. 1987, Lugo and Scatena 1996).

The second mortality component relates an individual's probability of mortality to its carbon balance. Studies in both tropical and temperate systems suggest

TABLE 2. Edaphic conditions at the six South American sites shown in Fig. 6 that were used to evaluate the size- and age-structured (SAS) approximation.

Site	Latitude, longitude	Monthly precip. (mm)			Soil depth (m)	Soil texture
		Mean	Max	Min		
Manaus (MN)	2°S, 61°W	188.4	406.8	54.8	2.5	fine
San Carlos (SC)	2°N, 68°W	212.0	294.3	122.3	2.5	medium
Paragominas (PA)	2°S, 48°W	227.0	455.7	63.8	2.5	medium
Santana (SA)	9°S, 51°W	134.8	292.3	4.8	2.5	fine
Calabozo (CB)	7°N, 70°W	162.0	339.5	8.7	1.2	medium
Caatinga (CA)	8°S, 48°W	55.3	209.7	0.4	2.1	fine/medium

Note: Mean, maximum, and minimum monthly precipitation (mm) obtained from the ISLSCP monthly precipitation data (see Appendix F) and soil depth (m) and texture class obtained from the ISLSCP soil characteristics database compiled by Koster et al. (Table 3; Meeson et al. 1995, Sellers et al. 1995) are shown.

that plants in prolonged low or negative carbon balance die quickly compared to plants in positive carbon balance, and that this source of mortality is an important determinant of the size structure of the forest understory (Augspurger and Kelly 1984, Kobe 1997). We included this form of mortality in the model, relating individual's probability of mortality to its current carbon balance. This component grades between high mortality for plants in low or negative carbon balance, to zero for plants in positive carbon balance. Its shape is governed by a single parameter, whose value is set to give reasonable understory size structure within forested grid cells. Details on the two components mortality functions are given in Appendix F.

Light

The incoming shortwave radiation from the climatological data is used to specify the PAR at the top of the gap canopy. The PAR within the canopy ($\phi(h, y, t)$) then decays exponentially as a function of the leaf area index above height (h), with a light extinction coefficient of 0.5 (Haxeltine and Prentice 1996). The light level of each plant is computed at the midpoint of its crown and assuming no overlap between the individual's crown and the crowns of taller and smaller individuals within the gap.

Soil hydrology

Early land-surface parameterization schemes represented soil moisture using simple equations for the moisture in the first few centimeters of soil (Sellers 1992). Vertically stratified soil moisture profiles and variation in plant rooting depths can cause problems with these simple ''bucket models'' (Koster and Milly 1997), and subsequently led to the development of schemes including variation in soil depth, multiple soil moisture layers, and sub-grid variability in infiltration capacity (Robock et al. 1996).

We model local (within-gap) soil moisture using a one-layer hydrology model with variable soil depth and texture. The precipitation rate is specified at the grid-cell level, however, sub-grid cell heterogeneity in water availability arises due to differences in evapotranspiration rates between gaps. Water losses due to percolation and runoff, are described using an empirical formulation for hydraulic conductivity as function of soil moisture content, soil depth, and soil texture (Campbell 1974). In this formulation, soil texture affects saturated water content, saturated hydraulic conductivity, and the rate at which conductivity decreases as saturation levels decrease (see Appendix G for details). The precipitation rate for each grid cell is input from the ISLSCP climatological data set, and soil depth and texture characteristics of each grid cell are specified from the ISLSCP soil characteristics data set (Tables 2 and 3).

TABLE 3. ISLSCP soil hydrology parameters (Meeson et al. 1995, Sellers et al. 1995).

Soil type	θ_{max}	K_{sat} (m/s $\times 10^{-6}$)	τ
Coarse	0.0363	14.1	4.26
Medium/coarse	0.1413	5.23	4.74
Medium	0.3548	3.38	5.25
Fine/medium	0.1349	4.45	6.77
Fine	0.263	2.45	8.17
Organic	0.354	3.38	5.25

Decomposition and nitrogen cycling

The Century model is a widely used model of belowground carbon and nitrogen dynamics (Parton et al. 1987, 1988, 1993, Potter et al. 1993, Schimel et al. 1994, 1996), and we employ a simplified version of it as our decomposition sub-model. While an understanding of the belowground dynamics of nitrogen and carbon is by no means complete, empirical studies have identified a number of general features that are included in Century and most other models of decomposition such as those in the FORTNITE and LINKAGES gap models (Aber et al. 1982, Post and Pastor 1996). These include the marked variation in decomposition times for different types of organic matter, the strong dependency of decomposition rates on soil temperature, moisture, and texture, and the coupling of the belowground carbon and nitrogen cycles. We follow the re-

sults of the analysis by Bolker et al. (1998), which shows that the Century model can be closely approximated by a model with five belowground compartments (quantitative details in Appendix H). We currently omit a number of phenomena important in some model applications including nitrogen fertilization, atmospheric nitrogen inputs, biological fixation, denitrification, leaching, and losses of nitrogen during fires.

Incoming litter is divided into fast (active) and slow (structural) pools of organic matter. The matter in each compartment decays exponentially, with a rate dependent on its lignin-to-nitrogen ratio, and on soil moisture, temperature, and texture. Under normal conditions in the tropics, the timescales of decomposition are approximately 0.5 yr for the fast compartment and 25 yr for the slow compartment.

When organic matter is mineralized, it releases its nitrogen to a plant-available belowground pool (nitrate and ammonium). Decomposition of the slow pool is halted if there is no available nitrogen (the decomposition of slow organic matter requires the input of mineralized nitrogen, Parton et al. (1987, 1993). However, in our model this rarely happens because it is superseded by an additional regulatory feedback; low available nitrogen reduces plant uptake, which reduces litter input.

Fire

Fire is a natural part of many ecosystems that can dramatically affect their composition, structure, and dynamics. In particular the location and structure of savannas are strongly influenced by the frequency and severity of fires (Neilson 1995). Many savannas burn with relatively high frequency, releasing carbon into the atmosphere and preventing succession to taller and woodier plant types (Kauffman et al. 1994).

There is a large body of literature on fire modeling and monitoring at local, regional, and continental scales (Rothermal 1972, 1991, Van Wagner 1977, Prinsm and Menzel 1992, Neilson 1995). The majority of fire models have two essential drivers: fuel and climate. The general dependence of fire frequency on these two quantities is highlighted by the prediction from many fire models that places of intermediate dryness have the highest burn rates, because very dry places are fuel-limited and wet places are climate-limited. The spatial spread of fire is also an important phenomenon. Continental-scale models, attempting to capture large-scale differences in fire regimes tend to assume homogeneous conditions and complete contagion within grid cells. In contrast, local and regional fire prediction models use detailed spatial information to predict the horizontal patterns of fire spread (Rothermal 1991).

We use a simple fire model comparable to that in Neilson's MAPSS ecosystem model (Neilson 1995) with the fire frequency within each grid cell being a simple function of fuel and climate. Unlike MAPSS, in our model burn rates are specified as a function of local fuel availability and local moisture conditions. We use local (within-gap) soil moisture as a dryness index for the local ignition of fires and the burn rate is assumed to be proportional to local fuel availability, defined simply as total aboveground biomass. The propagation of fires between gaps within a grid cell is modeled using the assumption that the landscape is fine-grained, which results in the burn rate of gaps being proportional to the total ignited fuel in the grid cell. We assume that burning consumes the aboveground vegetation completely. The belowground ecosystem is not directly affected; however a portion of the carbon released by the fire is loaded into the soil biogeochemical sub-model along with the nitrogen released during the fire. Details on the fire sub-model can be found in Appendix I.

Summary of the individual-based stochastic gap model

The above sub-models are implemented as a stochastic process in a series of simple steps. Suppose that a simulation of Q different gaps ($y = 1, 2, \ldots, Q$) is currently at time t and that we wish to produce the state of the system at time $t + \Delta t$. First, we grow each individual's structural stem in size by an amount $g_s(\mathbf{z}, \mathbf{x}, \mathbf{r}, t)\Delta t$ and each plant's living biomass by an amount $g_a(\mathbf{z}, \mathbf{x}, \mathbf{r}, t)\Delta t$. Here $\mathbf{r}$ is shorthand for the resource vector $\mathbf{r}(h, y, t)$, which has three elements: light, $\phi(h, y, t)$, water $W(y, t)$, and nitrogen $N(y, t)$. The growth functions integrate the output of the physiological and allometric sub-models, given local light, water, and nitrogen availability. The growth equations for structural and active tissues are given in Appendix E (Eqs. E.3 and E.4) . Second, we use the mortality sub-model to determine each plant's probability of mortality, $\mu(\mathbf{z}, \mathbf{x}, \mathbf{r}, t)\Delta t$, and kill the plant if a simulated pseudorandom coin toss with this probability indicates death. The mortality function $\mu(\mathbf{z}, \mathbf{x}, \mathbf{r}, t)\Delta t$, summarizes both sources of mortality and the equation is found in Appendix F (Eq. F.1). Third, each plant gives birth to an offspring with probability $f(\mathbf{z}, \mathbf{x}, \mathbf{r}, t)\Delta t$ (Eq. E.5 in Appendix E). New recruits are assigned to gaps at random. Fourth, we use the fire sub-model to calculate the probability of fire, $\lambda_F(y, t)\Delta t$, for each gap and toss simulated pseudorandom coins to determine which gaps burn (Eq. I.1 in Appendix I). Finally, we calculate, for each gap, the changes in the belowground amount of water ($W(y, t)$), soil carbon ($C_1(y, t)$ and $C_2(y, t)$), and soil nitrogen ($N_1(y, t)$, $N_2(y, t)$, and $N(y, t)$), using the hydrological and decomposition sub-models (Eqs. G.1 and H.1–H.5 in Appendices C and H, respectively).

Fig. 4a shows an example of output from the stochastic simulator for 25 linked gaps at San Carlos, a wet rain forest site. The output is obtained by using the above algorithm to simulate the carbon and nitrogen capture, water loss, growth, reproduction, and mortality of literally every individual throughout its life cycle

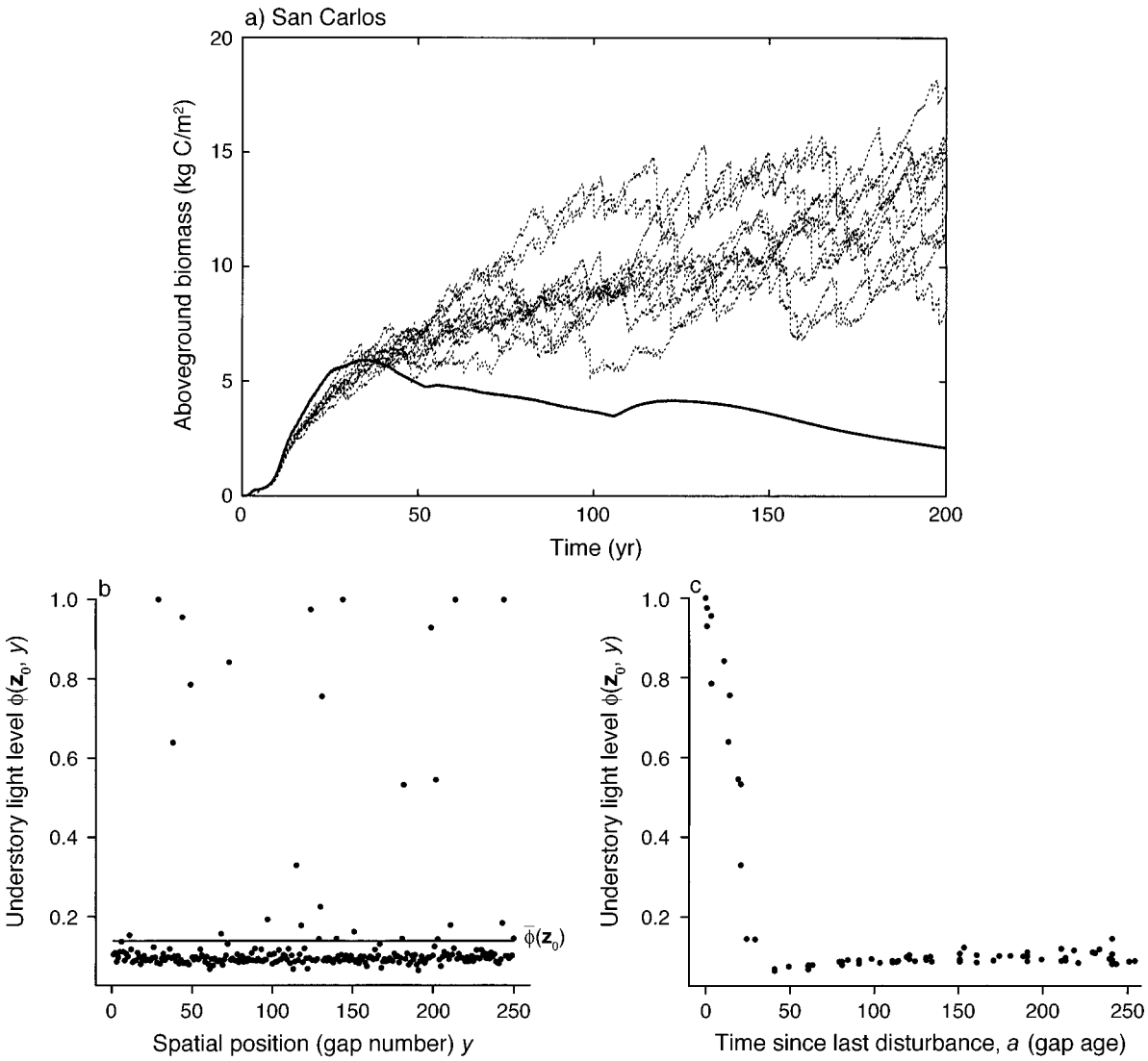

FIG. 4. (a) A 200-yr trajectory in aboveground biomass (kg C/m^2) at the San Carlos tropical forest site (2° N, 68° W), predicted by the ED model implemented as an individual-based stochastic gap model. The figure shows 10 runs of the stochastic process with each run containing 25 gaps (dashed lines). Also shown (solid line) is the trajectory predicted by a traditional size-structured approximation (Eqs. 11–13) of the stochastic gap model. (b) Distribution of understory light levels across gaps predicted by the model after the 200-yr integration shown in (a). The horizontal line shows the average light level at the bottom of the plant canopy $\bar{\phi}(\mathbf{z}_0)$ where size $\mathbf{z}_0$ corresponds to a height of 0.5 m. This spatially averaged (across-gap) light level is the effective understory light level in the traditional size-structured approximation of the stochastic gap model shown in (a). (c) Distribution of understory light levels $\phi(\mathbf{z}_0, y)$ in gaps shown in (a) plotted as a function of their time since last disturbance a. As this figure shows, the time since disturbance a accounts for most of the spatial (across-gap) variation in light levels shown in (b).

and the associated belowground dynamics of carbon, nitrogen, and water within each gap in the simulator.

SCALING

The model described in the previous section is a spatially distributed, nonlinear, stochastic process whose large-scale behavior we are interested in knowing. It is spatial because of the local nature of competition among plants for light, water, and nitrogen, nonlinear due to the nature of the relationships between local resource availability and a plant's growth, mortality, and recruitment rates, and stochastic because of the randomness of birth, dispersal, death, and disturbance.

The key to scaling such a model is the recognition that the ensemble average used for stand or landscape-level predictions is, in the limit of a large number of runs, the first moment of the stochastic process. We seek to formulate a differential equation that captures time-dependent behavior of this first moment while tak-

ing account of the variability in the model behavior that arises due to the stochastic nature of the processes operating in the model. A standard mathematical technique is to formulate a partial differential equation (PDE) that accounts for the variability in the stochastic process by capturing the dynamics of those processes that give rise to important heterogeneities in the ecosystem (Bailey 1964, Murray 1990, Levin and Pacala 1998).

In developing analytical versions of individual-based models of vegetation dynamics, a common initial strategy is to formulate a size-structured approximation that takes account of the size-related heterogeneity in light availability within the plant canopy (Okubo 1980, Pacala and Deutschman 1997). However, as we shall show, such size-structured approximations fail because in addition to the size-related vertical heterogeneity in light availability there is also a substantial degree of horizontal spatial heterogeneity in resource availability.

One approach to overcoming this problem of spatial heterogeneity in resource availability is to develop a second-order approximation, that takes account of the covariance that develops between local resource availability $\mathbf{r}(\mathbf{z}, y, t)$ (here a vector of local light, $\phi(\mathbf{z}, y, t)$, water $W(y, t)$, and nitrogen availability $N(y, t)$), and local plant density $n(\mathbf{z}, \mathbf{x}, y, t)$ (for example saplings of shade intolerant species are most abundant in locations with high light). This approach is often used in statistical physics where it is called ''Gaussian Random Fields.'' However, although the second order approximations work for some simple models of plant competition (Bolker and Pacala 1997, Levin and Pacala 1998, Pacala and Levin 1998; T. Kubo, *personal communication*), they are not generally useful due to instabilities arising from the omission of higher order terms and the large number of covariance equations necessary for approximating a functionally diverse plant community.

An alternative approach, which we use in our SAS approximation, is to identify, characterize, and then condition upon, events that are responsible for generating horizontal spatial heterogeneity in resource availability. To see this, let us first examine the behavior of the stochastic gap model.

Model simulations

We used the ED stochastic gap model defined in the *Model* section to simulate the ecosystem dynamics at San Carlos (SC) (2° S, 48° W), a tropical forest site in the Amazon region. The ensemble mean behavior of the model was characterized from 10 stochastic runs, each containing 25 gaps (25 15 $\times$ 15 m cells, $\sim$0.5 ha). Runs were initialized with a mean initial density of 0.1 seedlings (of size $\mathbf{z}_0$) per square meter of each of the four functional types, and run for 250 yr.

The trajectories of aboveground biomass (kilograms carbon per square meter) produced in the simulations show a considerable degree of variability between runs (dashed lines in Fig. 4a). Associated with the spatial heterogeneity in aboveground structure between runs is spatial between-gap variation in resource availability, in particular, variation in aboveground structure within each run. For example, (Fig. 4b) shows the between-gap variation in the understory light levels for each of the 250 gaps (25 $\times$ 10 runs) at year 200.

The traditional size-structured approximation fails because while it accounts for the vertical stratification in the light environment caused by plant shading, it does not account for the substantial degree of endogenous spatial heterogeneity in light availability between gaps (Fig. 4b). In the traditional size-structured approximation, the spatial variation in light profiles is averaged into a single mean light profile. For example, the line in Fig. 4b shows the light level assumed to be present in all gaps at a height of 0.5 m in the size-structured approximation. This light level is too low to allow regeneration to keep pace with canopy mortality, and so the size-structured approximation under-predicts the biomass in the simulator (solid line in Fig. 4a; see also Pacala and Deutschman 1997).

Two stochastic processes are responsible for generating most of the spatial heterogeneity in resource availability within the simulator. In tropical forest areas such as San Carlos, the majority of the spatial variation in light availability is associated with the mortality of large canopy trees. To see this, suppose we nominally define a canopy tree as any individual $>$10 m in height. Suppose further that for each spatial position (gap) y within the gap simulator, we record the time since the last stochastic canopy tree death, and call this event a disturbance event, and the time since the last such event, the age a of the gap. If we then plot light availability within each gap as a function of its age, we see a clear pattern in the distribution of light environments (Fig. 4c), which is responsible for most of the between-gap scatter shown in Fig. 4b. The second source of heterogeneity is fire, which is responsible for most of the spatial heterogeneity resource availability in arid areas where they occur.

The SAS approximation takes account of both the horizontal spatial heterogeneity and size-related heterogeneity. It captures horizontal heterogeneity by keeping track of a, the time since the last death of large adult tree or disturbance event. More formally, we develop a size-structured approximation for the ensemble mean conditional on age a. The derivation of this conditional approximation is facilitated by a subtle change in the way we view the stochastic events within the model. Gap simulators work because the size of a modeled gap is similar to the size of a large tree's crown (Botkin et al. 1972*b*, Shugart and West 1977). This ensures that single canopy tree deaths cause the high resource levels needed for rapid regeneration, and also cause gaps to contain at most one large tree. Suppose that we now replace the per-individual random coin

tosses that cause mortality in the simulator, with a per-place coin toss with the same probability, but only for trees above a threshold height h^*. That is, we continue to toss pseudorandom coins for each individual shorter than height h^* with probability of mortality μ, and toss a single coin with the same probability for the entire gap. If this toss indicates mortality, then we kill every tree in the gap taller than h^*. Because there is typically at most one such tree (if h^* is 10–15 m or larger), this change has no effect on the predictions of the stochastic process, as simulations confirm. However, because large tree deaths are now exogenous place-centered events, we can treat canopy tree deaths like other place-centered disturbances in the model such as fires. As Fig. 4c suggests, by conditioning appropriately on the occurrence of disturbance events and keeping track of the changing distribution of ages a since disturbance, we can account for the horizontal and vertical heterogeneity in resource availability they introduce.

Size- and age-structured (SAS) approximation

In this section, we derive the size- and age-structured (SAS) approximation for the first moment of the stochastic process within a grid cell. The derivation of the PDEs for this moment approximation is inevitably mathematical and readers not interested in the technical details may skip to *Evaluation of the moment equations* in which we evaluate the ability of the PDEs to capture the behavior of the stochastic gap simulator.

In the SAS approximation, we use the new variable to indicate the time since the most recent disturbance of any type (either fire or windthrow). Note however in principle, could be a vector, with each element denoting the time since the last event of a particular disturbance type. We begin by placing the individuals present within each gap y into a three-dimensional grid of bins, each of size Δz_s, Δz_a, and Δa. Let $U(\mathbf{z}, \mathbf{x}, a, y, t)$ be the number of individuals of type $\mathbf{x}$ in the yth gap that are between z_s and $z_s + \Delta z_s$ and between z_a and $z_a + \Delta z_a$ conditional on the gap having been disturbed between a and $a + \Delta a$ years ago. Note that $U(\mathbf{z}, \mathbf{x}, a, y, t)$ is a random variable whose value differs each time we simulate the stochastic process. If we let Δz_s, z_a, and $\Delta a \to 0$, $U(\mathbf{z}, \mathbf{x}, a, y, t)$ becomes a Bernoulli random variable (takes the value of either zero or one), and thus corresponds to the model described in the *Model* section implemented as a stochastic process (Fig. 5).

Now consider an infinite ensemble of runs of the stochastic process (the ensemble's probability density function). Let the operator $\langle\rangle$ be the mean value for all realizations of the stochastic process sharing the same $\mathbf{z}$, $\mathbf{x}$, y, t and a. We now define $u(\mathbf{z}, \mathbf{x}, a, y, t)$ as the conditional mean:

$$u(\mathbf{z}, \mathbf{x}, a, t) = \langle U(\mathbf{z}, \mathbf{x}, a, y, t)\rangle. \quad (1)$$

Note that this is the mean density of type $\mathbf{x}$ and size $\mathbf{z}$ plants in gaps of age (i.e., the local mean density conditional on age a) rather than the global density of plants across gaps of all ages. Note also that we have dropped the gap index y because we assume translational invariance, i.e., that the stochastic process is identical across all gaps within the same grid cell. We seek an equation for the change in the conditional ensemble mean over time (Δu).

Before defining an expression for Δu, we must redefine the transition probabilities of the stochastic gap model in accordance with the new rules governing disturbance (i.e., the h^* assumption). Let $\mu(a, \mathbf{x}, \mathbf{r}, t)\Delta t$ be the probability of mortality from density-dependent causes and, for plants shorter than h^*, from nonfire density-independent causes. Also, let $\lambda_{DI}(a, y, t)\Delta t$ be the probability of a density-independent disturbance within a gap that kills canopy trees taller than h^* and let $\lambda(a, y, t) = \lambda_F(a, y, t) + \lambda_{DI}(a, y, t)$, where $\lambda_F(a, y, t)\Delta t$ is the probability of fire. Finally, we define $s(h, a, t)$ as a step function equal to $\lambda_{DI}(a, y, t)$ for $h < h^*$, and $s(h, a, t) = 0$ otherwise.

Using this new notation, $\Delta u(\mathbf{z}, \mathbf{x}, a, t)$ is given by

$$\begin{aligned}
&\Delta u(\mathbf{z}, \mathbf{x}, a, t) \\
&= -\left\langle U(\mathbf{z}, \mathbf{x}, a, y, t) g_s(\mathbf{z}, \mathbf{x}, \mathbf{r}, t)\frac{\Delta t}{\Delta z_s}\right\rangle \\
&\quad + \left\langle U(\mathbf{z} - \Delta\mathbf{z}_s, \mathbf{x}, a, y, t) g_s(\mathbf{z} - \Delta\mathbf{z}_s, \mathbf{x}, \mathbf{r}, t)\frac{\Delta t}{\Delta z_s}\right\rangle \\
&\quad - \left\langle U(\mathbf{z}, \mathbf{x}, a, y, t) g_a(\mathbf{z}, \mathbf{x}, \mathbf{r}, t)\frac{\Delta t}{\Delta z_a}\right\rangle \\
&\quad + \left\langle U(\mathbf{z} - \Delta\mathbf{z}_a, \mathbf{x}, a, y, t) g_a(\mathbf{z} - \Delta\mathbf{z}_a, \mathbf{x}, \mathbf{r}, t)\frac{\Delta t}{\Delta z_a}\right\rangle \\
&\quad - \left\langle U(\mathbf{z}, \mathbf{x}, a, y, t)\frac{\Delta t}{\Delta a}\right\rangle + \left\langle U(\mathbf{z}, \mathbf{x}, a - \Delta a, y, t)\frac{\Delta t}{\Delta a}\right\rangle \\
&\quad - \langle U(\mathbf{z}, \mathbf{x}, a, y, t)\mu(\mathbf{z}, \mathbf{x}, \mathbf{r}, t)\Delta t\rangle \qquad (2)
\end{aligned}$$

where $\Delta\mathbf{z}_s$ is the vector $(\Delta z_s, 0)$ and $\Delta\mathbf{z}_a$ is the vector $(0, \Delta z_a)$. Note that g and μ are themselves random variables since they depend on $\mathbf{r}$, the vector containing the values light, water, and nitrogen, which are influenced by the presence or absence of individuals in the gap.

The first term on the right-hand side of Eq. 2 describes the ensemble average rate at which individuals grow out of size category z_s. The expression inside the brackets gives the average probability that a type $\mathbf{x}$, size $\mathbf{z}$ individual will grow into the next stem size-box during the time interval between t and $t + \Delta t$ given the values of the random variables. The ensemble expectation $\langle\rangle$ converts this probability into the average rate for the ensemble. Similarly, the second term describes the average rate at which type $\mathbf{x}$ individuals grow into the z_s stem size-box. The third and fourth terms describe the changes in the size of an individual's active pool (transport in z_a), and the fifth and sixth terms describe the aging of the gap in which the individual is present (transport in a) . The final term describes the loss due to mortality. Three of these terms are shown schematically in Fig. 5.

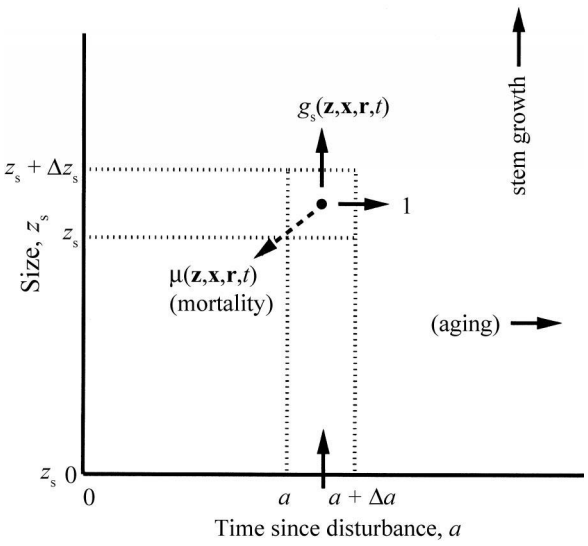

FIG. 5. Schematic representation of three stochastic processes occurring within the individual-based stochastic gap model that is used to formulate Eq. 2. Stem growth and aging are transport processes that move individuals in the size–age ($\mathbf{z}_s$, a) state space (indicated by solid lines), occurring at rates g_s and 1z, respectively (aging occurs at rate 1 since aging is a linear process with the same units as time). Mortality, occurring at rate μ involves the removal of individuals from the ($\mathbf{z}_s$, a) state space, so this is a loss term (indicated by dashed line).

Three technical problems presented by Eq. 2 are that (1) the g's and μ's are nonlinear functions, (2) the U's are statistically dependent due to the influence of other individuals on resources $\mathbf{r}$, which affects the values of the g's and μ's in Eq. (2), and (3) we lack an expression for the ensemble probability density.

The SAS approximation is obtained by Taylor expanding the expressions inside the brackets on the right-hand side of Eq. 2 about the size- and gap age-specific conditional ensemble means, neglecting second and higher order terms, and then dividing by Δt

$$\begin{aligned}\frac{\Delta u}{\Delta t} = &-\frac{1}{\Delta \mathbf{z}_s}[g_s(\mathbf{z}, \mathbf{x}, \bar{\mathbf{r}}, t)u(\mathbf{z}, \mathbf{x}, a, t) \\ &\quad - g_s(\mathbf{z}_s - \Delta \mathbf{z}_s, \mathbf{x}, \bar{\mathbf{r}}, t)u(\mathbf{z}_s - \Delta \mathbf{z}_s, \mathbf{x}, a, t)] \\ &- \frac{1}{\Delta \mathbf{z}_a}[g_a(\mathbf{z}, \mathbf{x}, \bar{\mathbf{r}}, t)u(\mathbf{z}, \mathbf{x}, a, t) \\ &\quad - g_a(\mathbf{z}_a - \Delta \mathbf{z}_a, \mathbf{x}, \bar{\mathbf{r}}, t)u(\mathbf{z}_a - \Delta \mathbf{z}_a, \mathbf{x}, a, t)] \\ &- \frac{1}{\Delta a}[u(\mathbf{z}, \mathbf{x}, a, t) - u(\mathbf{z}, \mathbf{x}, a - \Delta a, t)] \\ &- \mu(\mathbf{z}, \mathbf{x}, \bar{\mathbf{r}}, t)u(\mathbf{z}, \mathbf{x}, a, t) \qquad (3)\end{aligned}$$

where $\bar{\mathbf{r}}$ is the conditional ensemble average of resources for gaps of age a.

Defining $n(\mathbf{z}, \mathbf{x}, a, t) = u(\mathbf{z}, \mathbf{x}, a, t)/\Delta \mathbf{z} \Delta a$ and taking the limit $\Delta \mathbf{z}, \Delta a, \Delta t \to 0$ yields the following partial differential equation (PDE):

$$\begin{aligned}\frac{\partial}{\partial t}n(\mathbf{z}, \mathbf{x}, a, t) = &-\frac{\partial}{\partial z_s}[g_s(\mathbf{z}, \mathbf{x}, \bar{\mathbf{r}}, t)n(\mathbf{z}, \mathbf{x}, a, t)] \\ &- \frac{\partial}{\partial z_a}[g_a(\mathbf{z}, \mathbf{x}, \bar{\mathbf{r}}, t)n(\mathbf{z}, \mathbf{x}, a, t)] \\ &- \frac{\partial}{\partial a}n(\mathbf{z}, \mathbf{x}, a, t) \\ &- \mu(\mathbf{z}, \mathbf{x}, \bar{\mathbf{r}}, t)n(\mathbf{z}, \mathbf{x}, a, t). \qquad (4)\end{aligned}$$

change in plant density; growth in stem; growth in active tissue; aging of plant community; mortality

In addition, we require an equation for the probability distribution of age states a. Let $p(a, t)$ be the distribution of times since disturbance. Recalling that disturbances are occurring at rate $\lambda(a, t)$ and then using a similar approach to that described above, we can derive a PDE for the dynamics of $p(a, t)$, the age structure of the ecosystem within the grid cell:

$$\frac{\partial}{\partial t}p(a, t) = -\frac{\partial}{\partial a}p(a, t) - \lambda(a, t)p(a, t)$$

change in age structure; aging; disturbance

and

$$\int_0^\infty p(a, t)\, da = 1. \qquad (5)$$

The first term describes the aging process while the second $\lambda(a, t)$ term gives the rate at which areas of age a are disturbed. Eq. 5 is the von Foerster age distribution equation (von Foerster 1959).

For the case of random dispersal between gaps within a grid cell the recruitment of new seedlings $f(\mathbf{z}, \mathbf{x}, a, t)$ corresponds to a flux of individuals into the system at ($\mathbf{z}_0$, a) giving the following Neumann boundary condition

$$\begin{aligned}&n(\mathbf{z}_0, \mathbf{x}, a, t) \\ &= \left[\int_0^\infty \int_{\mathbf{z}_{0s}}^\infty \int_{\mathbf{z}_{0a}}^\infty n(\mathbf{z}, \mathbf{x}, a, t) f(\mathbf{z}, \mathbf{x}, a, t) p(a, t)\, d\mathbf{z}_a\, d\mathbf{z}_s\, da\right] \\ &\quad \times [g_a(\mathbf{z}_0, \mathbf{x}, \bar{\mathbf{r}}, t) + g_s(\mathbf{z}_0, \mathbf{x}, \bar{\mathbf{r}}, t)]^{-1}.\end{aligned}$$

recruitment

(6)

Eq. 4 also has a second boundary condition, describing

the state of the ecosystem following a disturbance event:

$$n(\mathbf{z}, \mathbf{x}, 0, t) = \underbrace{\int_0^\infty s(h(\mathbf{z}, \mathbf{x}), a, t)n(\mathbf{z}, \mathbf{x}, a, t)p(a, t)\, da}_{\text{plant community following disturance event}}. \quad (7)$$

Again, $h(\mathbf{z}, \mathbf{x})$ is the height of a plant of type $\mathbf{x}$ and size $\mathbf{z}$. The fraction of newly disturbed areas $p(0, t)$ is given by the boundary condition

$$p(0, t) = \underbrace{\int_0^\infty \lambda(a, t)p(a, t)\, da}_{\text{formation of newly disturbed areas}}. \quad (8)$$

We complete the size- and age-structured approximation by specifying initial conditions for Eqs. 4 and 5 corresponding respectively to the initial age distribution of areas within the grid cell and the size distribution of the plant types within each of these areas:

$$\underbrace{n(\mathbf{z}, \mathbf{x}, a, 0) = n_0(\mathbf{z}, \mathbf{x}, a)}_{\text{initial plant community}} \quad (9)$$

$$\underbrace{p(a, 0) = p_0(a)}_{\text{initial age distribution}}. \quad (10)$$

The PDEs (Eqs. 4 and 5) and their associated boundary (Eqs. 6–8), and initial conditions (Eqs. 9 and 10) describe the dynamics of a size- and age-structured plant community within a grid cell Ω, where $n(\mathbf{z}, \mathbf{x}, a, t)$ is formally the expected density of plants of size $\mathbf{z}$ and type $\mathbf{x}$ in a gap of age a at time t.

Following precisely the same steps used to derive the PDEs above, we also derive equations for the belowground water, carbon, and nitrogen conditional on age a (i.e., equations for $dW(a, t)/dt$, $dC_1(a, t)/dt$, $dC_2(a, t)/dt$, and $dN_1(a, t)/dt$, $dN_2(a, t)/dt$, $dN(a, t)/dt$, given by Eqs. G.2 and H.11–H.15 in the Appendices.

Note that size- and age-structured PDEs similar to Eqs. 4 and 5 have been used previously to model forest dynamics (Kohyama 1993, Kohyama and Shigesada 1995); however in these studies, the equations were formulated at the stand level rather than as an approximation to an individual-based model. The stand-level equations in these studies would approximate individual-based models if the appropriate changes were made to the mortality functions (the h^* assumption).

The size-structured approximation for individual-based models (Okubo 1980, Pacala and Deutschman 1997) is derived in the same way as Eq. 4 except that one expands about the mean density independent of age a obtaining

$$\underbrace{\frac{\partial}{\partial t}n(\mathbf{z}, \mathbf{x}, t)}_{\text{change in plant density}} = \underbrace{-\frac{\partial}{\partial \mathbf{z}_s}[g_s(\mathbf{z}, \mathbf{x}, \bar{\mathbf{r}}, t)n(\mathbf{z}, \mathbf{x}, t)]}_{\text{growth in stem}} - \underbrace{\frac{\partial}{\partial \mathbf{z}_a}[g_a(\mathbf{z}, \mathbf{x}, \bar{\mathbf{r}}, t)n(\mathbf{z}, \mathbf{x}, t)]}_{\text{growth in active tissues}} - \underbrace{[\mu(\mathbf{z}, \mathbf{x}, \bar{\mathbf{r}}, t) + \lambda(t)]n(\mathbf{z}, \mathbf{x}, t)}_{\text{mortality and disturbance}} \quad (11)$$

with the single boundary condition

$$\underbrace{n(\mathbf{z}_0, \mathbf{x}, t) = \frac{\int_{\mathbf{z}_{0s}}^\infty \int_{\mathbf{z}_{0a}}^\infty n(\mathbf{z}, \mathbf{x}, t)f(\mathbf{z}, \mathbf{x}, \bar{\mathbf{r}}, t)\, d\mathbf{z}_a\, d\mathbf{z}_s}{g_a(\mathbf{z}_0, \mathbf{x}, \bar{\mathbf{r}}, t) + g_s(\mathbf{z}_0, \mathbf{x}, \bar{\mathbf{r}}, t)}}_{\text{reproduction}} \quad (12)$$

and initial condition

$$\underbrace{n(\mathbf{z}, \mathbf{x}, 0) = n_0(\mathbf{z}, \mathbf{x})}_{\text{initial plant community}}. \quad (13)$$

Note that in the size-structured approximation (Eq. 11), $\bar{\mathbf{r}}$ is the spatially-averaged (nonlocal) resource condition within the grid cell.

Numerical Analysis

We solved the PDEs (Eqs. 4 and 5) numerically using the method of characteristics. The advective and quasi-linear nature of plant growth and aging terms in Eqs. 4 and 5 means that, by placing the PDEs in an appropriate moving frame of reference, it is possible to eliminate the flux terms, reducing the PDEs to systems of loosely coupled, ordinary differential equations that are easier and faster to solve (Murray 1990; P. R. Moorcroft, *unpublished data*).

Evaluation of the Moment Equations

We examined the ability of the SAS approximation (Eqs. 4 and 5) to correctly predict the ensemble mean behavior of the individual-based simulator at six sites representing a range of environmental conditions across tropical South America (Fig. 6). These sites were chosen to span gradients in total rainfall, rainfall seasonality, and soil type and depth that give rise to the range of community types found across the region (Table 2). They range from the evergreen wet forests at San Carlos, Venezuela and Manaus, Brazil, and seasonal wet forest at Paragominas, Brazil, to savannas on shallow soils at Calabozo, Venezuela, and on deep soil at Santana, Brazil, and a steppe (Caatinga, Brazil)

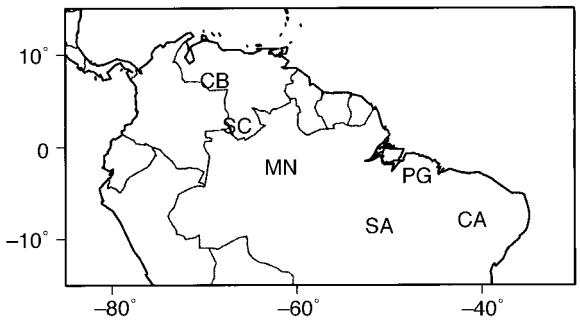

FIG. 6. Map showing the South American model region and the locations of the six model evaluation sites. Details of their rainfall, seasonality, and soil type are given in Table 2. San Carlos (SC), Venezuela, and Manaus (MN), and Paragominas (PG), Brazil, are tropical forest sites; Santana (SA), Brazil, and Calabozo (CB), Venezuela, are tropical savannas; and Caatinga (CA), Brazil, is an arid steppe.

site. As before, we characterized the ensemble mean behavior of the plant simulator at each site by performing 10 realizations of the stochastic process, simulating 25 15 × 15 m gaps for 200 years, and starting from a mean initial density of seedlings/m^2 (of size $\mathbf{z}_0$) per functional type.

Fig. 7a–f demonstrates that, unlike the traditional size-structured approximation, the SAS approximation captures the ensemble means across a wide range of conditions. Note that the SAS approximation of total aboveground carbon (red) predicts the center of the ensemble of stochastic runs (green) in all climates from very dry to very wet, and from strongly to weakly seasonal. In subsequent sections, we show that the SAS approximation also accurately predicts the ensemble means of the biomass of each functional type.

RESULTS

Regional results

We used the SAS approximation to implement ED over a region of tropical and subtropical South America (15° N to 15° S latitude) using ISLSCP I climate and soil data as inputs as described previously. We ran the model for all 1° × 1° grid cells in this region. In this section, we present and attempt to evaluate several model predictions about potential vegetation over the region. Evaluating biosphere models at this scale is difficult however, since regional data are not available for most of the model state variables and predicted fluxes. For this reason, our presentation and evaluation of model predictions at the regional scale will be cursory. In the next section we evaluate the model's predictions in greater detail at several local sites where more data are available.

To evaluate the model's behavior across the region, we assembled three sources of regional information on three model predictions: carbon in live biomass, soil carbon, and mean annual net primary production (NPP). For live biomass, we compare model predictions to data from the Olson et al. (1983) global database (Fig. 8). This database was constructed from information on vegetation distributions, stand characteristics, and patterns of human land use. It consists of a global map, at 1° × 1° resolution, of the average density (kilograms carbon per square meter) of carbon in live vegetation. For soil carbon, we use the RADAM dataset (de Negreiros and Nepstad 1994), which includes soil profiles from over 1100 natural sites in the Brazilian Amazon (Fig. 9). Finally, for NPP we compare our model predictions to those of the Miami model (Lieth 1972) (Fig. 10). The Miami model is an empirical model relating mean annual net primary production to mean annual temperature and precipitation. Each of these data sets, and the Miami model, are widely known to the ecosystem community and have been used in the evaluation of ecosystem models.

For each of these characteristics (carbon in live vegetation, soil C, and mean annual NPP), we provide a four-panel figure comparing the model and the regional information (Fig. 8–10). Each figure includes: a map of our model predictions (panel a), a map of the information we are comparing to (panel b), a map of the differences between the two (panel c), and a histogram of the mapped differences (panel d). First, note from panel d in each of these figures that there is generally close agreement between model predictions and the regional information. Each of the histograms of the differences between the regional information and the model predictions has a mode near zero. Second, note that many of the spatial patterns of above- and belowground carbon storage and NPP across the region are also captured by the model (panels a–c of Figs. 8–10). For example, in Fig. 8 one can see the low biomass grassland region of the Orinoco Llanos, the large forested region of Amazonia with high biomass, the Atlantic coastal tropical forest, the comparatively low biomass region of the dry Caatinga in the Southeast, and the deserts along the Pacific coast.

There are also areas of disagreement. The model predicts high values of soil organic matter in the northwestern part of the Amazon basin (Fig. 9). Though it is difficult to evaluate the significance of this feature since there is little overlap with the data set, the RADAM data for adjoining areas do not show the same spatial trend as the model. The high predicted values in the northwestern portion of the basin result from the influence of soil moisture on decomposition rates in the Century decomposition formulation. High soil moisture in these areas causes a sharp decline in decomposition rate, leading to a buildup of soil organic matter (Appendix H).

Also, despite the approximately zero mode of differences between the model predictions and the Olsen aboveground biomass data, there are also some areas of conspicuous disagreement (Fig. 8 panel c, and the large shoulder on the right of panel d). Some of the low values of aboveground biomass are isolated pixels within the Amazon region that reflect anomalous soil

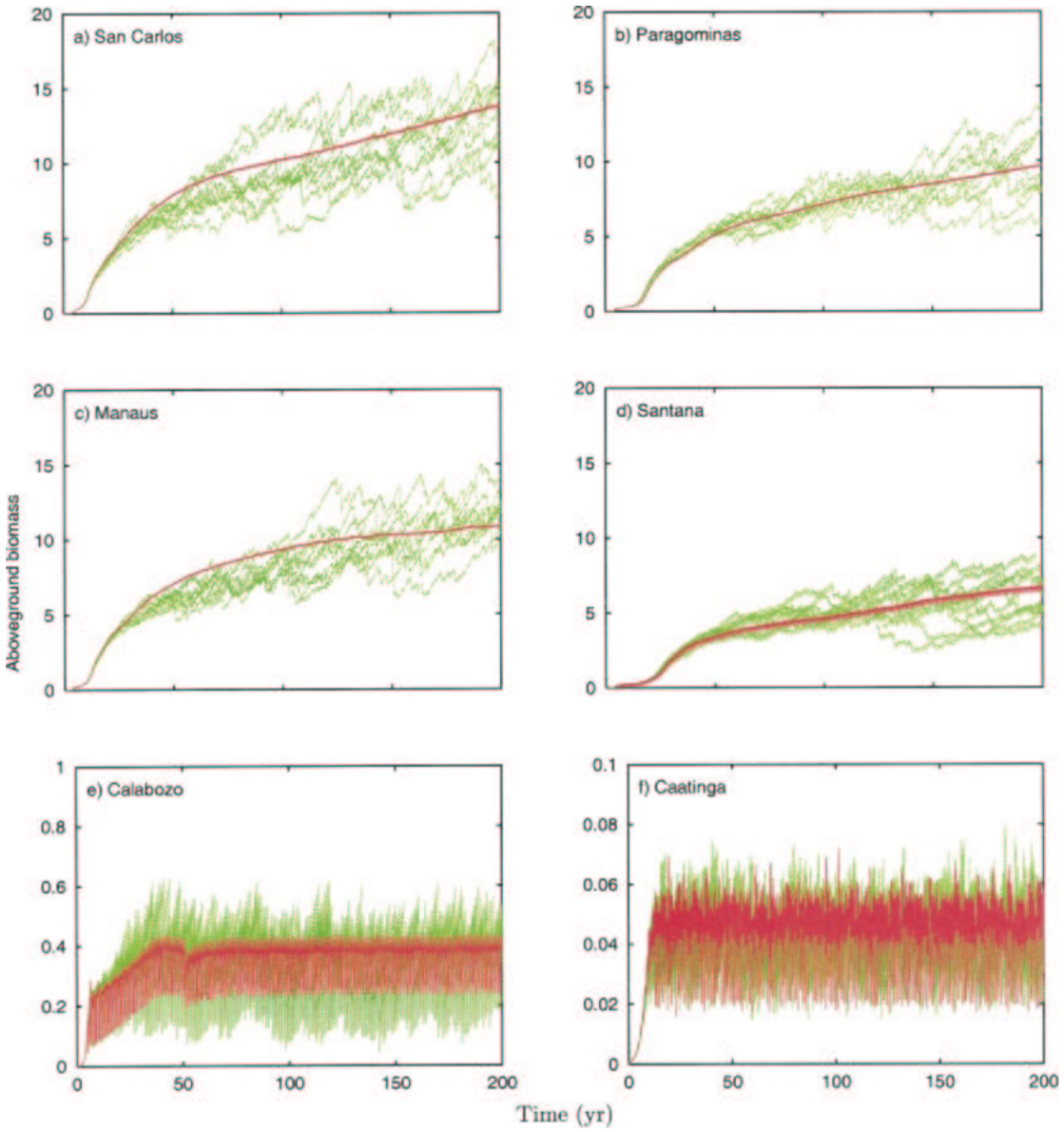

FIG. 7. Trajectory of aboveground biomass (kg C/m^2) at the (a) San Carlos (SC), (b) Paragominas (PG), (c) Manaus (MN), (d) Santana (SA), (e) Calabozo (CB), and (f) Caatinga (CA) sites as output by 10 runs of ED implemented as a stochastic gap model (green lines) and the size–age structured (SAS) approximation (Eqs. 4 and 5, red line). The locations of San Carlos and other evaluation sites are shown in Fig. 6.

characteristics in the ISLSCP data set (panel a). Panels b and c illustrate that discrepancies also occur along the boundaries between biomes. These are not surprising given that the location of biome boundaries is challenging to predict, since they reflect a change in the outcome of plant competition along transition zone. However, this cannot account for the large number of grid cells for which our model over-predicts the aboveground carbon data (panels c and d). These occur predominantly in the South and Southeast portions of Brazil, regions of known intensive human land use. The predominance of agriculture in these areas tends to lower aboveground biomass below its natural state by removing trees and other forms of woody vegetation and replacing them with crops.

To move beyond the level of regional model–data comparison offered here will require more comprehensive data sets and a model that accounts for human land use. Without these, it is difficult to determine whether anomalies and differences between regional model predictions and regional data are due to model inaccuracies or the absence of processes such as human land use within the model. For this reason, we now turn to more detailed local comparisons at three selected sites.

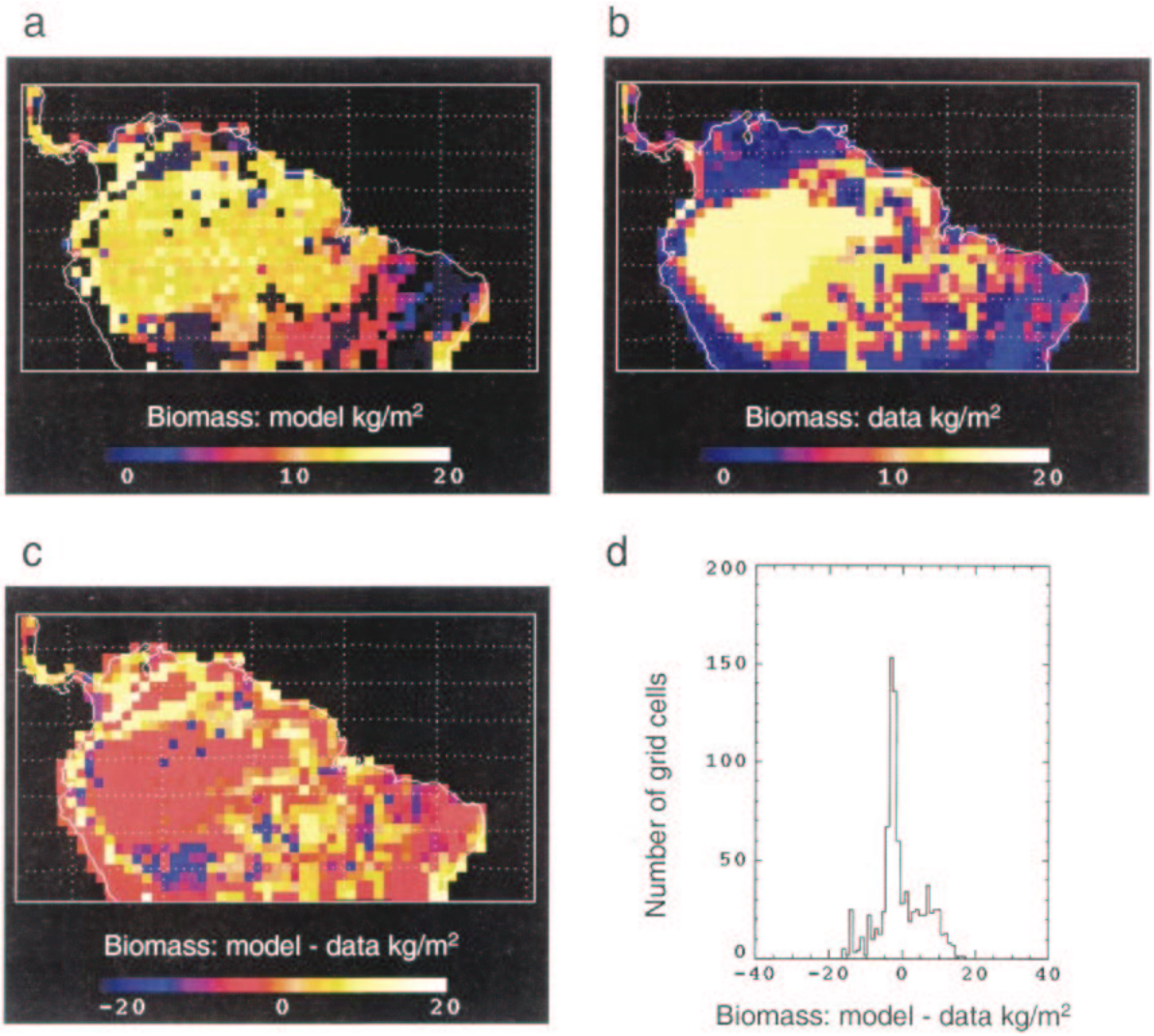

FIG. 8. Model predictions of average biomass compared to Olson et al. (1983) data on biomass (kg C/m²). (a) Model predictions of average biomass after 200-yr regional model integration using the SAS partial differential equations (PDE). (b) Olson et al. (1983) data on biomass. (c) A map of the difference between (a) and (b). (d) A histogram of the differences (measured in kg C/m²) mapped in (c). The vertical axis is the number of grid cells in each bin. The Olson et al. (1983) data set includes the effects of human land use, which may explain the differences between the data and model predictions in the south and southeast portions of Brazil.

San Carlos: patterns of forest succession

San Carlos is the evergreen rain forest site at which the chronosequence of aboveground biomass shown in Fig. 1 was collected. Does our biosphere model correctly predict the observed long timescale of carbon accumulation at San Carlos? If so, then what mechanisms cause the delay? And are these the same mechanisms that occur in nature?

The pattern of accumulation exhibited by our model closely resembles the observed trajectory of aboveground biomass recorded in the 200-yr chronosequence at San Carlos (Fig. 11a). Biomass accumulation is initially rapid, with ~6–8 kg C/m² of accumulation during the first 30–50 yr. Then after this initial period of rapid increase, aboveground biomass accumulates more slowly, gaining a further 6–7 kg C/m² over the next 150–170 yr and reaching 13 kg C/m² after 200 yr (Fig. 11a).

The mechanism responsible for this 200-yr timescale and pattern of biomass accumulation is the same in the model and observations. As Saldarriaga et al. (1988) note in their paper, the rapid initial biomass increase during the first 50 yr is caused by colonization by fast-growing early successional trees with low wood density that rapidly form a closed forest canopy. Aboveground biomass then continues to accumulate for the next 150 yr, albeit more slowly, due to gradual replacement of the early successional trees with slower growing, mid- and late successional trees with higher wood density.

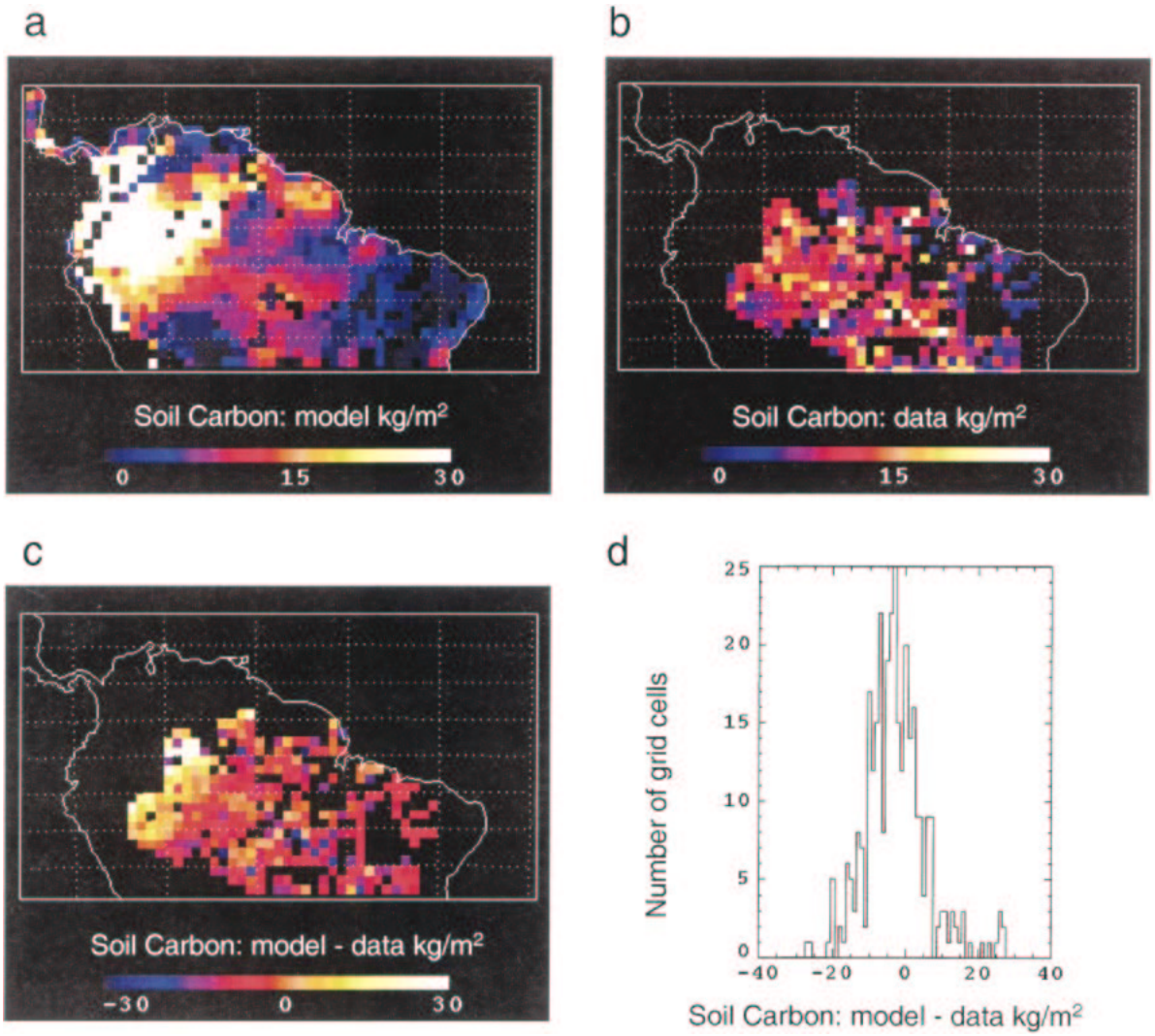

FIG. 9. Model predictions of average soil carbon stocks (kg C/m^2) compared to RADAM (de Negreiros and Nepstad 1994) data on soil carbon. (a) Predicted soil carbon ($C_1 + C_2$) after 200-yr regional model integration using the SAS PDEs. (b) RADAM soil carbon estimates calculated by combining RADAM soil-profile data on soil type and percentage soil carbon content with average soil-type-dependent bulk-density values from the literature (Potter et al. 1998) to estimate depth-integrated soil-carbon stocks (C. Kucharik, *personal communication*). The values plotted above are the average of the RADAM values within each 1° grid cell. (c) A map of the differences between the values plotted in (a) and the data in (b). (d) A histogram of the differences (measured in kg C/m^2) mapped in (c). The vertical axis is the number of grid cells in each bin.

The pattern and timescale of aboveground biomass succession at San Carlos predicted by our model arises from a similar successional process (Fig. 11b). After a short period in which grasses briefly proliferate, early successional tree growth dominates biomass accumulation during the first 50 yr. This is followed by slower biomass accumulation as the early successional trees are competitively replaced by slower growing mid- and late successional trees with higher wood densities. Note also that the SAS approximation shown in Fig. 11b accurately predicts the ensemble average for each functional type obtained from stochastic simulations of ED. These runs are the same as those used to produce the pattern of total aboveground biomass in Fig. 7a.

The importance of competitive successional dynamics in determining the timescale of aboveground biomass accumulation at San Carlos is made apparent by comparing the trajectory of biomass accumulation when the plant types compete, forming a heterogeneous mixed stand, to the biomass trajectory of each species run separately and allowed to form monospecific stands (Fig. 11c). In the monospecific stand of the early successional species, initial biomass accumulation is rapid, but asymptotes below the chronosequence observations. In the monospecific stand of the late successional species, biomass accumulates more slowly and equilibrates far above the chronosequence observations (Fig. 11c). The biomass trajectory of a monospecific

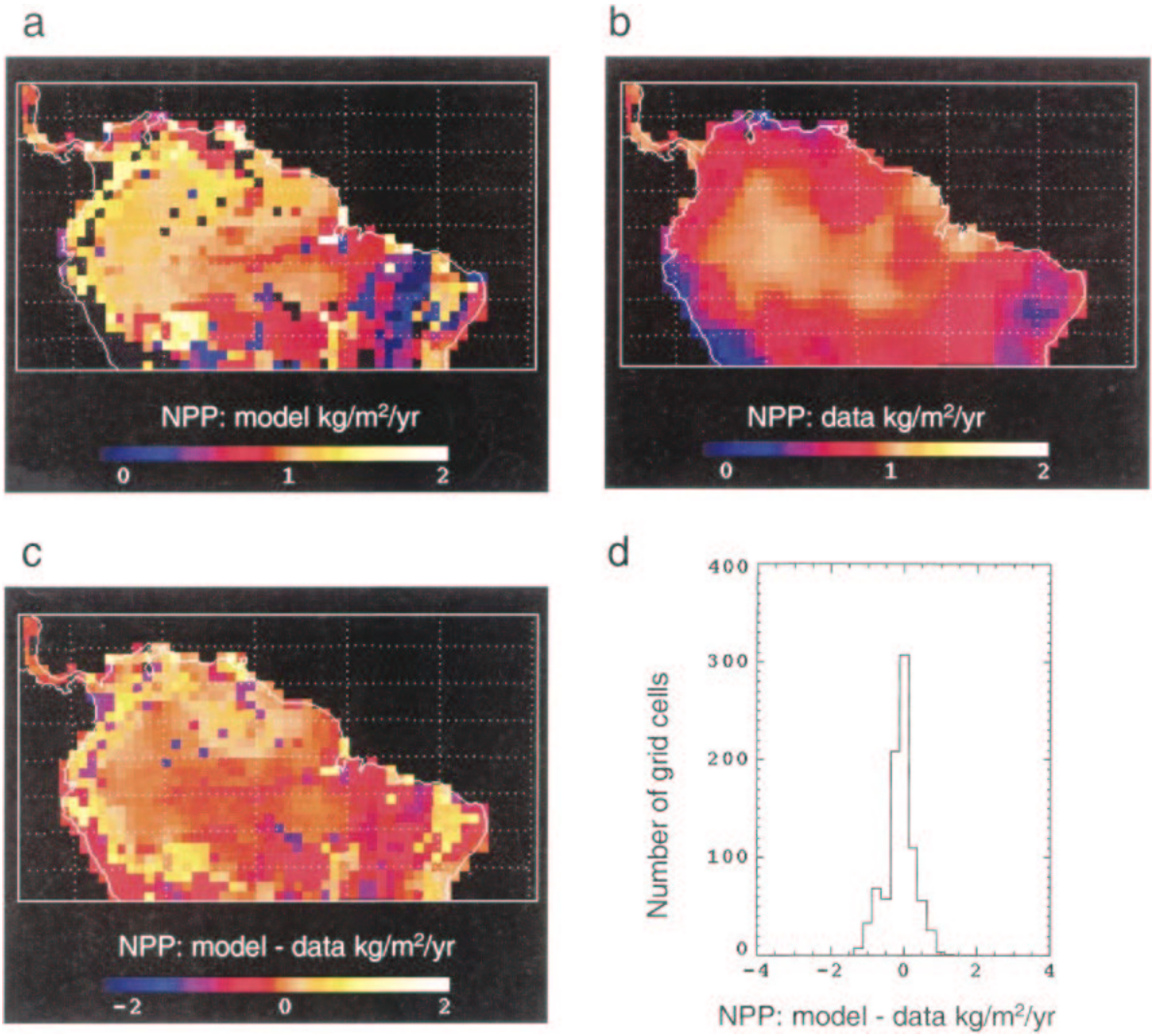

FIG. 10. Model predictions of average net primary production (NPP) compared to the Miami model (Lieth 1972). (a) Predicted average annual aboveground NPP (kg C·m^{-2}·yr^{-1}). Values were computed by averaging the monthly aboveground NPP values obtained from the 200-yr regional model integration using the SAS PDEs. (b) Miami model average annual aboveground NPP (kg C·m^{-2}·yr^{-1}), assuming a carbon-to-biomass ratio of 0.5. The Miami model estimates were calculated using the same annual temperature and precipitation data used in (a). (c) A map of the differences between (a) and (b). (d) A histogram of the differences (measured in kg C/m^2) in (c). The vertical axis is the number of grid cells in each bin.

stand of the mid-successional species follows the chronosequence observations more closely; however, the timescale of biomass accumulation in the monospecific stand is faster than the mixed stand and the chronosequence observations (Fig. 11c).

In summary, two processes produce the long timescale of succession at San Carlos in both the observations and our model. First, height-structured competition allows fast growing but short-lived trees to forestall domination of the forest by higher wood density species for a century or so. These high wood density species are relatively long-lived and thus grow to large average size and store large amounts of carbon. Second, a further century or so is required before the average size of late successional trees stops increasing. Thus, the first mechanism is at the community level (temporary competitive suppression of the eventual dominant), while the second is at the population level (the time required for the formation of a stable size and age distribution of the late successional dominant). Also, it is important to understand that sub-grid scale heterogeneity is essential to matching the predicted and actual patterns at San Carlos. The traditional size-structured approximation, which lacks horizontal heterogeneity caused by sub-grid scale disturbance, severely under-predicts the trajectory of aboveground biomass at San Carlos (compare Figs. 1 and 4a).

The PDEs for the San Carlos grid cell equilibrate approximately by year 500 with 18 kg C/m^2 above ground. At equilibrium, the C_4 grass species is absent

but the pioneer, mid- and late successional trees are all present (Fig. 11d). In recently disturbed gaps (ages between 0 and 40 yr), aboveground biomass is relatively low and dominated by the low wood density early successional pioneer species. However in older gaps, the aboveground biomass is considerably higher and the early successional pioneers have been replaced by mid- and late successional trees with higher wood densities (Fig. 11d).

The size structure of the different functional types across the range of gap ages at year is shown in Fig. 11e. Each of the elements in the figure is a characteristic from the numerical solution of the PDEs. Aboveground biomass in the areas with gap ages between 0 and 40 yr is concentrated in the small size classes, consisting primarily of saplings of the early successional pioneer forest trees. In gaps between 40 and 120 yr old, these saplings of the early successional species have grown rapidly to form an initial canopy of larger size class trees. Due to their low wood density, these initial large size classes do not contain a substantial amount of aboveground biomass; and beneath is a midstory of saplings of the mid- and late successional tree species. Aboveground biomass in gaps that have remained undisturbed for long periods of time (120–200 yr) is much higher, the initial canopy of early successional pioneers having been replaced by large-sized mid- and late successional trees with higher wood densities. The mid-story beneath these large size-class late successionals is relatively empty (Fig. 11e).

Calabozo: the role of fire in the formation and maintenance of savanna communities

Calabozo is a savanna in the Orinoco Llanos dominated by C_4 grasses and with interspersed trees. The site receives considerably less rainfall than San Carlos and has a more pronounced dry season, accentuated by the shallow soil, which limits the soil moisture field capacity (Table 2). The savannas of the Llanos burn frequently, with short fire return times (Mueller-Dombois and Goldhammer 1990), preventing development of substantial woody biomass and leading to equilibrium aboveground carbon stores of 0.1–0.9 kg C/m^2 (Jose and Medina 1976, Jose and Farinas 1983), many times less than at San Carlos.

Fig. 12a shows that the model predicts the coexistence of C_4 grasses and short leaf life span early successional trees, with an equilibrium biomass within the correct range. Note also, that the SAS approximation captures the ensemble dynamics of the individual functional types obtained from stochastic simulations at Calabozo (Fig. 12b). Unlike San Carlos, the dry season at Calabozo is severe enough to drive soil moisture beneath the threshold for fires to occur. The high frequency oscillations in the figure reflect seasonal variation in the availability of soil water from the hydrology model and the occurrence of dry-season burns. The fire regime develops in the model together with the ecosystem (Fig. 12c) . Initially, the aboveground biomass within the grid cell is low so fires occur infrequently; however fire frequency increases as biomass accumulates within gaps, increasing local fuel availability. Eventually, the ecosystem and disturbance regime come into equilibrium, with an exponential distribution of times since fire and most gaps having a short return-time between fires (Fig. 12d).

At equilibrium, the region is composed of a mosaic of gaps. In gaps burned within the past five years, aboveground biomass is low and dominated by grasses with interspersed tree seedlings (Fig. 12e, f). In a small proportion of older areas that have escaped fire for several years, aboveground biomass is higher and dominated by trees with reduced biomass beneath (Fig. 12e, f). The important point here is that the mixed grass–tree savanna formation at Calabozo is caused in the model by sub-grid scale heterogeneity associated with fire.

Manaus: role of sub-grid scale heterogeneity in tropical forest net ecosystem productivity

In this section we return to the second example in the *Introduction* regarding the importance of sub-grid scale processes to interpreting eddy-correlation measurements of NEP. Specifically we examine the pattern of sub-grid scale heterogeneity in NEP predicted by the model at Manaus (MN, see Fig. 6). After 500 yr, the grid-cell level net primary productivity and total belowground respiration of the Manaus ecosystem come close to equilibrium, yielding an approximately ''balanced biosphere'' with an NEP of 0.1 kg $C \cdot m^{-2} \cdot yr^{-1}$.

Examination of the pattern of sub-grid scale heterogeneity underlying this approximate balance shows that it arises from a statistical equilibrium between gaps within the grid cell that are in positive carbon balance and other areas that are in negative carbon balance (Fig. 13). Gaps that have been recently disturbed (recent canopy tree death) are rapidly losing large amounts carbon, while gaps with ages $>$20 yr since a canopy tree death gain carbon at a rate of 0.2–0.3 kg $C \cdot m^{-2} \cdot yr^{-1}$, equivalent to 2–3 metric tons of carbon per hectare annually.

The grid-cell level NEP value of 0.1 kg $C \cdot m^{-2} \cdot yr^{-1}$ is given by the integral of the relationship shown in Fig. 13 between NEP and successional age over the age distribution for the grid cell from Eq. 5. Eddy-flux tower measurements of NEP will correctly measure this integral if disturbances among gaps are not spatially correlated, because it will sample a sufficiently large number of statistically independent gap-sized areas. However, if disturbances are correlated at large spatial scales, say because of synoptic weather events or infrequent large-scale fires, then a tower is likely to produce a strongly nonzero measurement of NEP even though the regional average is close to zero.

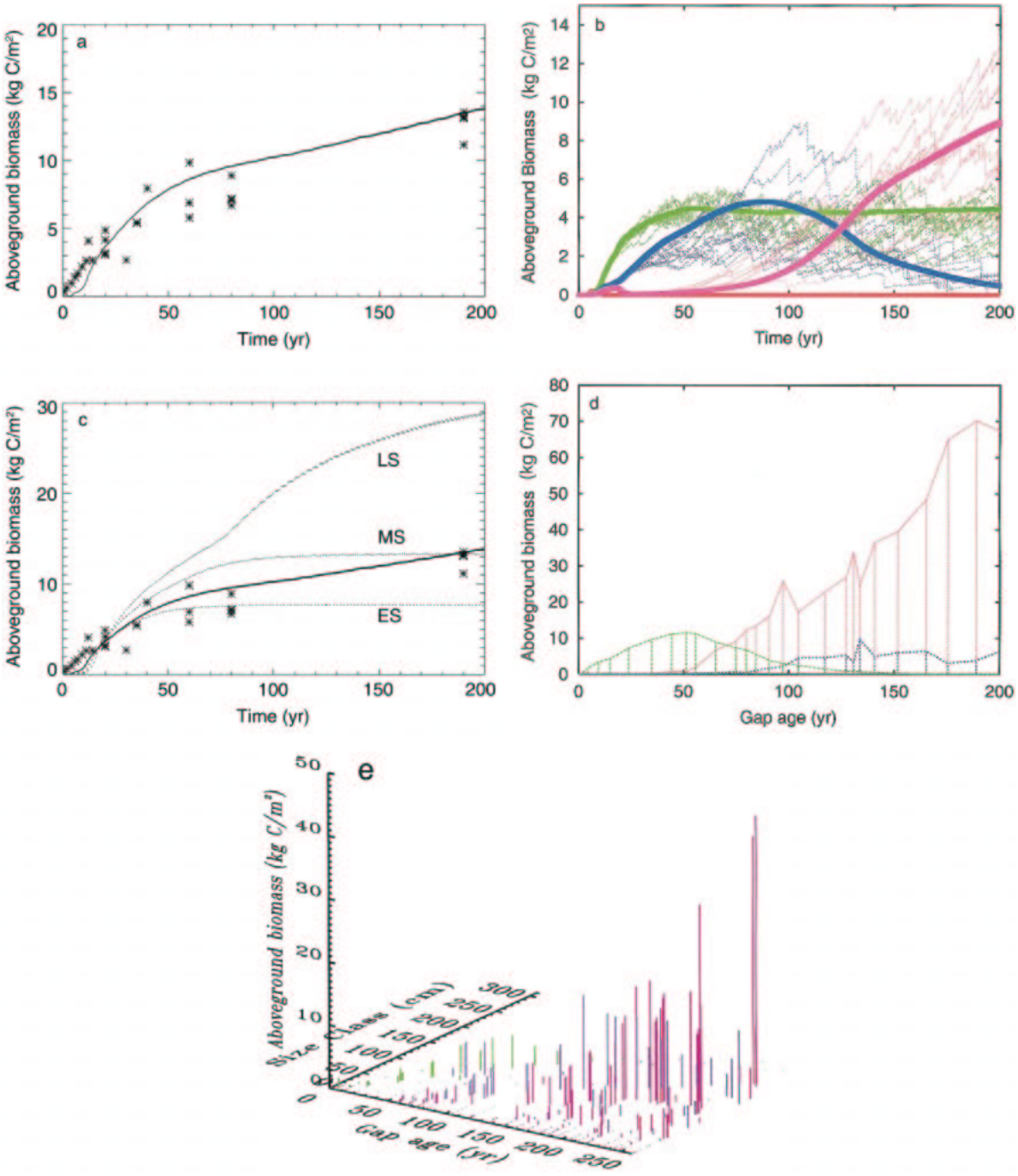

FIG. 11. (a) Trajectory of aboveground biomass (kg C/m²) at San Carlos predicted by the ED model compared to the chronosequence of aboveground biomass measurements made by Uhl (1987) and Saldarriaga et al. (1988). (b) Forest composition changes at the San Carlos tropical forest site underlying the trajectory of aboveground biomass shown in (a). Thin lines show the trajectories of aboveground biomass of C_4 grass (red), early successional trees (green), mid-successional trees (blue), and late successional trees (pink) predicted by the ED model implemented as an individual-based stochastic gap simulator. Thick lines show the corresponding trajectories from an SAS approximation. (c) Aboveground biomass trajectories (kg C/m²) for monospecific stands at the San Carlos tropical forest site predicted by the model. Dotted lines show monospecific stands of the early (ES), mid (MS), and late (LS) functional tree types. The solid line shows the corresponding trajectory for the heterogeneous stand shown in (a). Points are the chronosequence data collected by Uhl (1987) and Saldarriaga et al. (1988). (d) The equilibrium composition of aboveground biomass (kg C/m²) at San Carlos as a function of gap age *a* (yr). In recently disturbed areas, aboveground biomass is composed mostly of early successional trees (green lines) while in older areas aboveground biomass is dominated by the late successional tree functional type (pink lines). (e) Sub-grid scale heterogeneity in aboveground biomass at the San Carlos tropical forest site predicted by the model. Vertical lines show the

Discussion

The predictions of ED illustrate the advantages of formulating ecosystem models at the scale of individual plants. Individual-based ecosystem models naturally capture the fine-scale population and community-level processes responsible for the slow timescale of carbon uptake in aggrading tropical forest, the mix of trees and grasses in savanna, and the distribution of local NEP values about the grid-cell average. These and related factors explain the continued successes of individual-based ecosystem models over the past 30 years (Huston et al. 1988, Huston 1992, Shugart and Smith 1996). Also, because the model is formulated at a scale consistent with field studies, the model is comparatively easier to parameterize and test with data collected at finer scales (Huston et al. 1988, Pacala et al. 1996). For example, as we showed in this paper, the abundant data on allometry of individual trees can be used to constrain ecosystem-level allocation, and forest inventory data can be used to test the model's predictions about forest composition, stand structure, and carbon storage. In addition, many forms of satellite data are now approaching resolutions consistent with formulating fine-scale models of the biosphere.

Compared to traditional formulations that are parameterized and tested at a single spatial scale, the ability of fine-scale formulations to connect to data collected at a variety of scales is also likely to improve confidence in large-scale predictions, which are often difficult to test directly. For example, our model predicts many of the details of ecosystem dynamics at San Carlos and Calabozo including successional transients, and has regional predictions of NPP and aboveground carbon and soil carbon that are generally consistent with the limited regional data available. However, areas of disagreement point to necessary improvements in future versions of ED. For example, the predictions of soil organic matter in the northwest portion of the Amazon basin are probably too high due to inadequacies in our treatment of the effects of soil moisture on decomposition. The discrepancies in aboveground carbon values in the Southeast probably result from the absence of human land use in the model. The significance of mismatches at this scale is difficult to evaluate however, as the regional estimates themselves are subject to a high degree of error and uncertainty.

The most general contribution of our study is the scaling methods that provide the PDEs for predicting ensembles of gap-model runs. We suspect that these will work for any individual-based simulator of vegetation. The physical environmental sciences rely fundamentally on directly analogous scaling technologies. Modern atmospheric and oceanic GCMs typically rely on PDEs rather than stochastic Lagrangian particle simulators for reasons of computational efficiency and because their compactness permits mathematical analysis. The scaling that leads from the individual-based gap model to our size- and age-structured (SAS) approximation is analogous to that leading from a stochastic Lagrangian particle simulator to the Navier-Stokes equations.

The fundamental difference between the Navier-Stokes equations and the SAS PDEs is that rules governing the underlying stochastic process are completely understood for the former, but still very much under development for the latter. We emphasize that the individual-based model introduced in this paper is only one of many possible formulations for a stochastic gap model driven by ecophysiological and biogeochemical mechanisms. Our model is a member of the class founded by the Hybrid model (Friend et al. 1997); similar models are under development by a variety of groups.

The success of the SAS approximation in capturing the dynamics of the corresponding stochastic gap model implies that ecosystem dynamics at the grid-cell scale depend critically on the size structure and the local disturbance history (age distribution) at sub-grid scales. This point is further emphasized by the success of the SAS approximation at San Carlos and Calabozo, where field data confirm the critical role of sub-grid scale processes in large-scale ecosystem structure and dynamics. It also confirms the findings of earlier work using stochastic gap models, which showed the importance of disturbances such as fire and windthrow in influencing the structure and composition of plant communities (Doyle 1981, Noble and Slatyer 1981, Shugart and Seagle 1985).

Since the information regarding the long-term behavior of stochastic gap model resides in the sub-grid cell heterogeneity of the SAS approximation, we can view the three components of sub-grid cell variability: size structure, age structure, and functional type composition, as embodying the long-term memory of the aboveground ecosystem, which determines its subsequent dynamics. As a result, the ability to characterize and understand the size-related, age-related, and com-

---

←

size distribution of aboveground biomass of the early (green), mid (blue), and late (pink) successional tree functional types and how this changes as a function of time since last disturbance (gap age a in years). Plant sizes are shown in diameter (cm) values while aboveground biomass values are shown in units of kg C/m^2. The horizontal (x–y) position of the lines reflects the characteristics that constitute the numerical solution of the SAS PDE (Eq. 4). The figure illustrates that the aboveground biomass in recently disturbed areas is composed mostly of small-sized trees of the early-successional type (green lines). In areas of intermediate age, aboveground biomass is composed of mid-sized trees of all three functional tree types. In old undisturbed areas (high a), aboveground biomass is dominated by large-sized trees of late-successional functional type (pink lines).

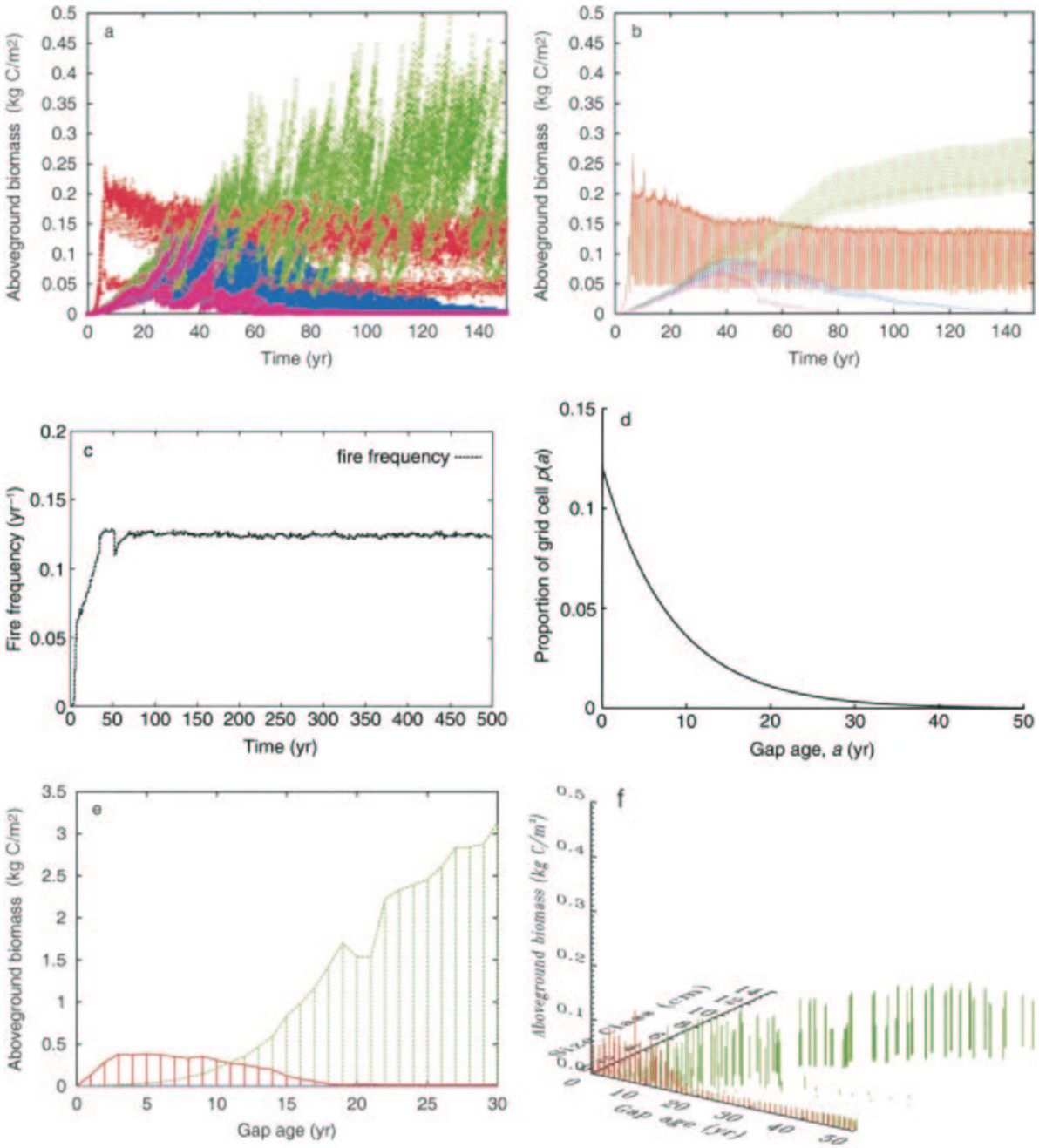

FIG. 12. (a) Formation and maintenance of a mixed grass–tree community at the Calabozo (CB) tropical savanna site as output from 10 runs of ED implemented as a stochastic gap model. The figure shows the aboveground biomass trajectory (kg C/m^2) for each plant functional type: C_4 grasses (red lines), and early (green), mid (blue), and late (pink) successional tree types. (b) Aboveground biomass trajectories (kg C/m^2) for the plant functional types at Calabozo (CB) predicted by an SAS approximation of the stochastic gap model. The pattern of community composition predicted by the SAS approximation closely approximates that of the corresponding stochastic simulations shown in (a). (c) Temporal development of a fire disturbance regime at Calabozo in the Orinoco Llanos responsible for the formation and maintenance of a grass–tree savanna shown in (a) and (b). The figure shows the total disturbance rate $\lambda(t)$ given by the current fire disturbance rate $\lambda_F(a, t)$ (Eq. I.1 [in Appendix I]) plus the rate of windthrow disturbance $\lambda_{DI}(a, t) = 0.014$ yr^{-1} (Eq. F.3 [in Appendix F]) summed over the current age distribution $p(a, t)$ (given by the solution of Eq. 5). (d) Age structure of the Calabozo tropical savanna ecosystem predicted by the SAS approximation. The figure shows the equilibrium distribution of gap ages $p(a)$ given by the solution of Eq. 5. The equilibrium disturbance rate $\lambda(t) = 0.12$ yr^{-1} corresponds to an average fire return time of ~8 yr. (e) Sub-grid scale heterogeneity ecosystem structure at Calabozo tropical savanna as a function of gap age (yr). The figure shows the distribution of aboveground biomass (kg C/m^2) of the plant functional types across gap ages following the 200-yr integration shown in (b). Note that the aboveground biomass in recently disturbed areas is composed mostly of C_4 grass (red lines), while older areas are dominated by trees with short-leaf lifespan (green lines). (f) Predicted sub-grid scale heterogeneity in

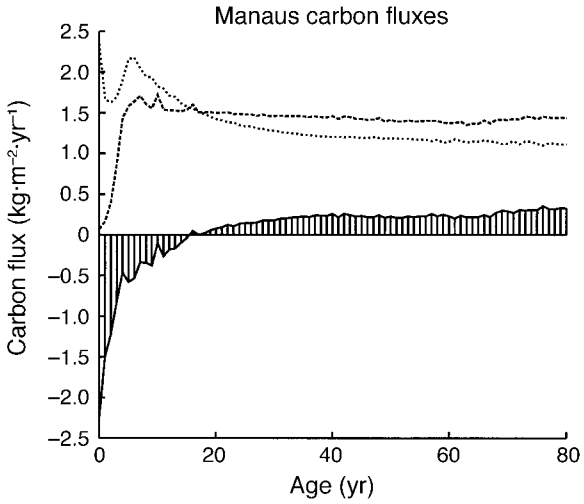

FIG. 13. Predicted variation in net ecosystem production (NEP; kg $C \cdot m^{-2} \cdot yr^{-1}$) as a function of gap age at Manaus following 500-yr model integration using the SAS PDEs. The shaded line shows NEP, while the dashed and dotted lines show respectively, the distributions of net primary productivity (NPP) and belowground heterotrophic respiration (r_h) across gap ages that underlie the age distribution of NEP (NEP = NPP − r_h). Despite the rapid recovery of NPP, recently disturbed gaps are in negative carbon balance because the aboveground material accumulated prior to disturbance is now decomposing, and as a result belowground respiration exceeds NPP. Older gaps are in positive carbon balance because belowground respiration declines beneath NPP as gaps age.

position-related structure of ecosystems is fundamental to a better understanding of their long-term fate. This further suggests that inventories of vegetation structure (e.g., Phillips et al. 1998), may hold the key to predicting the future large-scale dynamics of ecosystems, and provides additional incentive for satellite measurements of vegetation structure using Vegetation Canopy Lidar (VCL, Dubayah et al. 1997).

Use of the SAS approximation offers the same two principal advantages over direct simulation of stochastic gap models as the Navier-Stokes equations offer over Lagrangian particle simulators. First, the formulation obviates the need for many-run stochastic ensembles, thereby greatly reducing the computational burden (by one to several orders of magnitude). Accurate characterization of ensemble means through simulation can be a computationally intensive exercise. Although Friend et al. (1997) show that 10 runs of a single canopy gap may be sufficient in ideal circumstances, our experience suggests that the necessary number is often one to several orders of magnitude larger. For this reason, we found it necessary to simulate at least 250 gaps to characterize ensemble means in this paper (10 runs each with 25 gaps). If the size of the ensembles were too small, then one or more of the functional types that coexist in our simulations of evergreen rain forest at San Carlos would become extinct with high probability, and this would significantly alter the timescale of carbon accumulation following subsequent disturbance (Fig. 11a–e). The necessary size of an ensemble increases geometrically with the number of dimensions of heterogeneity that must be captured. Future studies may find it necessary to move beyond our formulation and include sub-grid scale heterogeneity in land-use, abiotic physical heterogeneities such as soils and topography, as well as other dimensions of functional diversity. Such applications will amplify the importance of the increase in computational efficiency offered by the SAS PDEs.

Second, like the Navier-Stokes equations, the SAS approximation offers the promise of increased understanding through mathematical analysis. Although analytically formidable, the SAS approximation is much more tractable than the stochastic gap model itself. We suspect that it will ultimately yield analytical insights about the connection between local ecosystem processes and large-scale ecosystem function.

ACKNOWLEDGMENTS

We gratefully acknowledge the generous support of the National Oceanic and Atmospheric Administration and the support of the National Aeronautics and Space Administration (LBA-Ecology grant NCC5-338 to B. Moore). We also acknowledge the support of the Department of Energy and the National Science Foundation. We thank Luis Solazarno for sharing his insights and observations of South American ecosystems and thank Simon Levin, Jorge Sarmiento, Ben Bolker, John Caspersen, Manuel Gloor, Elena Shevliakova, and Berrien Moore for suggestions and comments on the manuscript.

LITERATURE CITED

Aber, J. D., and J. M. Melillo. 1982. FORTNITE: a computer model of organic matter and nitrogen dynamics in forest ecosystems. University of Wisconsin Research Bulletin R3130. Madison, Wisconsin, USA.

Augspurger, C. K., and C. K. Kelly. 1984. Pathogen mortality of tropical tree seedlings: experimental studies of the effects of dispersal distance, seedling density and light conditions. Oecologia **61**:211–217.

Bailey, N. T. J. 1964. The elements of stochastic processes with applications to the natural sciences. Wiley, New York, New York, USA.

Baldocchi, D., and E. Falge. 1998. Report from the Second International FLUXNET workshop. Technical report. Atmospheric Turbulence and Diffusion Division, National

←

aboveground biomass at Calabozo following the 200-yr integration of the SAS approximation shown in (b). As in Fig. 11e, vertical lines show how aboveground biomass within the savanna is distributed across size classes and how this changes as a function of gap age *a*. Recently disturbed areas contain C_4 grasses (red lines) and a few small early successional trees (green lines), while older areas contain larger trees and a reduced biomass of C_4 grasses.

Oceanic and Atmospheric Administration, Oak Ridge, Tennessee, USA.

Baldocchi, D., R. Valentini, S. Running, W. Oechel, and R. Dahlman. 1996. Strategies for measuring and modelling carbon dioxide and water vapour fluxes over terrestrial ecosystems. Global Change Biology **2**:159–168.

Ball, J. T., I. E. Woodrow, and J. E. Berry. 1986. A model predicting stomatal conductance and its contribution to the control of photosynthesis under different environmental conditions. Volume 4. Martinus-Nijhoff, Dordrecht, Netherlands.

Bolker, B. M., and S. W. Pacala. 1997. Using moment equations to understand stochastically driven spatial pattern formation in ecological systems. Theoretical Population Biology **52**:179–197.

Bolker, B., S. W. Pacala, F. A. Bazzaz, C. D. Canham, and S. A. Levin. 1995. Species diversity and ecosystem response to carbon dioxide fertilization: conclusions from a temperate forest model. Global Change Biology **1**:373–381.

Bolker, B. B., S. W. Pacala, and W. J. Parton. 1998. Linear analysis of soil decomposition: insights from the CENTURY model. Ecological Applications **8**:425–439.

Bonan, G. B. 1989. A computer model of the solar radiation, soil moisture, and soil thermal regimes in boreal forests. Ecological Modelling **45**:275–306.

Bonan, G. B. 1995. Land-atmosphere CO_2 exchange simulated by a land surface process model coupled to an atmospheric general circulation model. Journal of Geophysical Research **100**(D2):2817–2831.

Botkin, D. B., J. F. Janak, and J. R. Wallis. 1972*a*. Rationale, limitations, and assumptions of a northeastern forest growth simulator. IBM Journal of Research and Development **16**: 101–116.

Botkin, D. B., J. F. Janak, and J. R. Wallis. 1972*b*. Some ecological consequences of a computer model of plant growth. Ecology **60**:849–873.

Bugmann, H. K. M. 1996. A simplified forest model to study species composition along climate gradients. Ecology **77**: 2055–2074.

Campbell, G. S. 1974. A simple method for determining unsaturated conductivity from moisture retention data. Soil Science **117**:311–314.

Clark, J. S., and Y. Ji. 1995. Fecundity and dispersal in plant populations: implications for structure and diversity. American Naturalist **146**:72–111.

Clark, J. S., E. Macklin, and L. Wood. 1998. Stages and spatial scales of recruitment limitation in southern Appalachian forests. Ecological Monographs **68**:213–235.

Coffin, D. P., and W. K. Lauenroth. 1990. A gap dynamics simulation model of succession in a semi-arid grassland. Ecological Modelling **49**:229–236.

Collatz, G. J., J. T. Ball, C. Grivet, and J. A. Berry. 1991. Physiological and environmental regulation of stomatal conductance, photosynthesis and transpiration: a model that includes a laminar boundary layer. Agricultural and Forest Meteorology **54**:107–136.

Collatz, G. J., M. Ribas-Carbo, and J. A. Berry. 1992. Coupled photosynthesis-stomatal conductance model for leaves of C_4 plants. Australian Journal of Plant Physiology **19**: 519–538.

de Negreiros, G. H., and D. C. Nepstad. 1994. Mapping deeply rooting forests of Brazilian Amazonia with GIS. Pages 334–338 *in* Proceedings of ISPRS Commission VII Symposium—Resource and Environmental Monitoring. Volume 7(a). Rio de Janeiro, Brazil.

Dickinson, R. E., A. Henderson-Sellers, and P. J. Kennedy. 1993. Biosphere–Atmosphere Transfer Scheme (BATS) Version 1e as Coupled to the NCAR Community Climate Model. Technical report. Technical Note Number 387. National Center for Atmospheric Research, Boulder, Colorado, USA.

Doyle, T. W. 1981. The role of disturbance in the gap dynamics of a montane rain forest: an application of a tropical forest succession model. Pages 56–73 *in* D. C. West, H. H. Shugart, and D. B. Botkin, editors. Forest succession. Concepts and application. Springer-Verlag, New York, New York, USA.

Dubayah, R., J. B. Blair, J. Bufton, D. Clark, J. JaJa, R. Knox, S. Luthcke, S. Prince, and J. Weishampel. 1997. The vegetation canopy lidar mission. Pages 100–112 *in* Proceedings of land satellite information in the next decade II: Sources and applications. American Society for Photogrammetry and Remote Sensing, Bethesda, Maryland, USA.

Farquhar, G. D., and T. D. Sharkey. 1982. Stomatal conductance and photosynthesis. Annual Review of Plant Physiology **33**:317–345.

Foley, J. A., I. C. Prentice, N. Ramankutty, S. Levis, D. Pollard, S. Sitch, and A. Haxeltine. 1996. An integrated biosphere model of land surface processes, terrestrial carbon balance, and vegetation dynamics. Global Biogeochemical Cycles **10**:603–628.

Friend, A. D., A. K. Stevens, R. G. Knox, and M. G. R. Cannell. 1997. A process-based, terrestrial biosphere model of ecosystem dynamics. Ecological Modelling **95**:249–287.

Haxeltine, A., and I. C. Prentice. 1996. Biome 3: an equilibrium terrestrial biosphere model based on ecophysiological constraints, resource availability, and competition among plant functional types. Global Biogeochemical Cycles **10**:693–709.

Haxeltine, A., I. C. Prentice, and I. D. Creswell. 1996. A coupled carbon and water flux model to predict vegetation structure. Journal of Vegetation Science **7**:651–666.

Hurtt, G. C., P. R. Moorcroft, S. W. Pacala, and S. A. Levin. 1998. Terrestrial models and global change: challenges for the future. Global Change Biology **4**:581–590.

Hurtt, G. C., and S. W. Pacala. 1995. The consequences of recruitment limitation: reconciling chance, history, and competitive differences between plants. Journal of Theoretical Biology **176**:1–12.

Huston, M. 1992. Individual-based forest succession models and the theory of plant competition. Pages 408–420 *in* D. L. DeAngelis and L. J. Gross, editors. Individual-based models and approaches in ecology. Routledge, Chapman and Hall, London, UK.

Huston, M. A., D. L. DeAngelis, and W. M. Post. 1988. New computer models unify ecological theory. Bioscience **38**: 682–691.

Huston, M. A., and T. M. Smith. 1987. Plant succession: life history and competition. American Naturalist **130**:168–198.

Kauffman, J. B., D. L. Cummings, and D. E. Ward. 1994. Relationships of fire, biomass and nutrient dynamics along a vegetation gradient in the Brazilian cerrado. Journal of Ecology **82**:519–531.

Kerr, Y. H. 1995. A review of the ISLSCP Initiative I CD-ROM collection: context, scope, and main outcome. Goddard Space Flight Center, National Aeronautics and Space Administration, Greenbelt, Maryland, USA.

Kittel, T. G. F., J. A. Royle, C. Daly, N. A. Rosenbloom, W. P. Gibson, H. H. Fisher, D. S. Schimel, L. M. Berliner, and VEMAP2 Participants. 1997. A gridded historical (1895–1993) bioclimate dataset for the conterminous United States: model input data for VEMAP phase 2. Pages 219–222 *in* Proceedings on the 10th Conference on Applied Climatology (Reno, Nevada, 20–24 October 1997). American Meteorological Society, Boston, Massachusetts, USA.

Kobe, R. 1997. Carbohydrate allocation to storage as a basis

of interspecific variation in sapling survivorship and growth. Oikos **80**:226–233.

Kohyama, T. 1993. Size structured tree populations in gap-dynamic forest—the forest architecture hypothesis for the stable coexistence of species. Journal of Ecology **81**:131–143.

Kohyama, T., and N. Shigesada. 1995. A size-distribution-based model of forest dynamics along a latitudinal environmental gradient. Vegetatio **121**:117–126.

Koster, R. D., and P. C. D. Milly. 1997. The interplay between transpiration and runoff formulations in land surface schemes used with atmospheric models. Journal of Climate **10**:1578–1591.

Lawton, R. O. 1984. Ecological constraints on wood density in a tropical montane rain forest. American Journal of Botany **71**:261–267.

Leuning, R. 1995. A critical appraisal of a combined stomatal-photosynthesis model for C_3 plants. Plant Cell and Environment **18**:339–355.

Levin, S. A., and S. W. Pacala. 1998. Theories of simplification and scaling in ecological systems. Pages 271–296 *in* D. Tilman and P. Kareiva, editors. Spatial ecology: the role of space in population dynamics and interspecific interactions. Princeton University Press, Princeton, New Jersey, USA.

Lieth, H. 1972. Modeling the primary productivity of the world. Nature and Resources **8**(2):5–10.

Lindner, M. 1999. Simulating forest development with alternative forest management strategies under climatic change—application of a forest gap model in risk analysis. Pages 5–13 *in* Forestry scenario modelling in risk analysis and management. European Forest Institute, Joensuu, Finland.

Lugo, A. E., and F. N. Scatena. 1996. Background and catastrophic tree mortality in tropical moist, wet and rain forests. Biotropica **28**:585–599.

Mann, L. K., and W. M. Post. 1980. Modelling the effect of drought on forest growth. Bulletin of the Ecological Society of America **61**:80.

Meeson, B. W., F. E. Corprew, J. M. P. McManus, D. M. Myers, J. W. Closs, K. J. Sun, D. J. Sunday, and P. J. Sellers. 1995. ISLSCP Initiative I—global data sets for land–atmosphere models, 1987–1988. American Geophysical Union, Washington, D.C., USA. [Available on CD-ROM.]

Melillo, J. M., A. D. McGuire, D. W. Kicklighter, B. Moore, C. J. Vorosmarty, and A. L. Schloss. 1993. Global climate change and terrestrial net primary production. Nature **363**: 234–239.

Morrill, J. C. 1999. Sensitivity of a land surface model to the diurnal distribution of downward longwave radiation. Journal of the Meteorological Society of Japan **77**:265–279.

Mueller-Dombois, D., and J. G. Goldhammer. 1990. Fire in tropical systems. Pages 51–72 *in* J. G. Goldhammer, editor. Fire in the tropical biota. Blackwell Science, Oxford, UK.

Murray, J. D. 1990. Mathematical biology. Springer-Verlag, Berlin, Germany.

Neilson, R. P. 1995. A model for predicting continental-scale vegetation distribution and water balance. Ecological Applications **5**:362–385.

Noble, I. R., and R. O. Slatyer. 1980. The use of vital attributes to predict successional changes in plant communities subject to recurrent disturbance. Vegetatio **43**:5–21.

Noble, I. R., and R. O. Slatyer. 1981. Concepts and models of succession in vascular plant communities subject to recurrent fire. Pages 311–335 *in* A. M. Gill, R. H. Groves, and I. R. Noble, editors. Fire and the Australian biota. Australian Academy of Science, Canberra, Australia.

Okubo, A. 1980. Diffusion and ecological problems: mathematical models. Volume 10. Biomathematics. Springer-Verlag, Basel, Germany.

Olson, J. S., J. A. Watts, and L. J. Allison. 1983. Carbon in live vegetation of major world ecosystems. Report ORNL-5862. Oak Ridge National Laboratory, Oak Ridge, Tennessee, USA.

Pacala, S. W., C. D. Canham, J. Saponara, J. A. Silander, R. K. Kobe, and E. Ribbens. 1996. Forest models defined by field measurements: estimation, error analysis and dynamics. Ecological Monographs **66**:1–43.

Pacala, S. W., and D. H. Deutschman. 1997. Details that matter: the spatial distribution of individual trees maintains forest ecosystem function. Oikos **74**:357–365.

Pacala, S. W., and S. A. Levin. 1998. Biologically generated spatial pattern and the coexistence of competing species. Pages 204–232 *in* D. Tilman and P. Kareiva, editors. Spatial ecology: the role of space in population dynamics and interspecific interactions. Princeton University Press, Princeton, New Jersey, USA.

Pacala, S. W., and D. Tilman. 1993. Limiting similarity in mechanistic and spatial models of plant competition in heterogeneous environments. American Naturalist **143**:222–257.

Parton, W. J., D. S. Schimel, C. V. Cole, and D. S. Ojima. 1987. Analysis of factors controlling soil organic matter levels in Great Plains grasslands. Soil Science Society of America Journal **51**:1173–1179.

Parton, W., J. Scurlock, D. Ojima, R. Scholes, D. Schimel, T. Gilmanov, T. Kirchner, J. C. Menaut, T. Seastedt, E. G. Moya, A. Kamnalrut, and J. Kinyamario. 1993. Observations and modeling of biomass and soil organic matter dynamics for the grassland biome worldwide. Global Biogeochemical Cycles **7**:785–809.

Parton, W., J. Stewart, and C. Cole. 1988. Dynamics of C, N, P and S in grassland soils: a model. Biogeochemistry **5**:109–131.

Pastor, J., and W. M. Post. 1985. Development of linked forest productivity–soil process model. Technical report TM-9519. Oak Ridge National Laboratory, Oak Ridge, Tennessee, USA.

Phillips, O. L., Y. L. Malhi, N. Higuchi, W. F. Laurance, P. V. Nunez, R. M. Vasquez, S. G. Laurance, L. V. Ferreira, M. Stern, S. Brown, and J. Grace. 1998. Changes in the carbon balance of tropical forests: evidence from long-term plots. Science **282**:439–442.

Pollard, D., and S. L. Thompson. 1995. Use of a land-surface-transfer scheme (LSX) in a global climate model: the response to doubling stomatal resistance. Global and Planetary Change **10**:129–161.

Post, W. M., and J. Pastor. 1996. LINKAGES—an individual based forest ecosystem model. Climate Change **34**:253–261.

Potter, C. S., E. A. Davidson, S. A. Klooster, and D. C. Nepstad. 1998. Regional application of an ecosystem production model for studies of biogeochemistry in Brazilian Amazonia. Global Change Biology **4**:315–333.

Potter, C. S., J. T. Randerson, C. B. Field, P. A. Matson, P. M. Vitousek, H. A. Mooney, and S. A. Klooster. 1993. Terrestrial ecosystem production: a process model based on global satellite and surface data. Global Biogeochemical Cycles **7**:811–841.

Prentice, I. C., W. Cramer, S. P. Harrison, R. Leemans, R. A. Monserud, and A. M. Solomon. 1992. A global biome model based on plant physiology and dominance, soil properties and climate. Journal of Biogeography **19**:117–134.

Prinsm, E. M., and W. P. Menzel. 1992. Geostationary satellite detection of biomass burning in South America. International Journal of Remote Sensing **13**:2783–2799.

Putz, F. E., P. D. Coley, A. Montalvo, and A. Aiello. 1983. Snapping and uprooting of trees: structural determinants

and ecological consequences. Canadian Journal of Forest Research **13**:1011–1020.

Reich, J. W., E. B. Rastetter, J. M. Melillo, D. W. Kicklighter, P. A. Steudler, B. J. Peterson, A. L. Grace, III, B. Moore, and C. J. Vorosmarty. 1991. Potential net primary productivity in South America: application of a global model. Ecological Applications **1**:399–429.

Reich, P. B., M. B. Walters, and D. S. Ellsworth. 1997. From tropics to tundra: global convergence in plant functioning. Proceedings of the National Academy of Sciences (USA) **94**:13730–13734.

Robock, A., C. A. Schlosser, K. Y. Vinnikov, S. Liu, and N. A. Speranskaya. 1996. Validation of humidity, moisture fluxes, and soil moisture in GCMs: report of AMIP diagnostic subproject 11. Part 1—soil moisture. Pages 85–90 *in* W. L. Gates, editor. Proceedings of the first international AMIP scientific conference WCRP-92, WMO/TD-Number 732. World Climate Research Programme, Geneva, Switzerland.

Rothermal, R. C. 1972. A mathematical model for predicting fire spread in wildland fuels. USDA Forest Service Research Paper **INT-115**.

Rothermal, R. C. 1991. Predicting behavior and size of crown fires in the Northern Rocky Mountains. USDA Forest Service Research Paper **INT-438**.

Saldarriaga, J. G., D. C. West, M. L. Tharp, and C. Uhl. 1988. Long-term chronosequence of forest succession in the upper Rio Negro of Colombia and Venezuela. Journal of Ecology **76**:938–958.

San Jose, J. J., and M. R. Farinas. 1983. Changes in tree density and species composition in a protected *Trachypogon* savannah, Venezuela. Ecology **64**:447–453.

San Jose, J. J., and Y. E. Medina. 1976. Organic matter production in the *Trachypogon* savanna at Calabozo, Venezuela. Tropical Ecology **17**:113–124.

Schimel, D. S., B. H. Braswell, E. A. Holland, R. McKeown, D. S. Ojima, T. H. Painter, W. J. Parton, and A. R. Townsend. 1994. Climatic, edaphic, and biotic controls over storage and turnover of carbon in soils. Global Biogeochemical Cycles **8**:279–293.

Schimel, D. S., B. H. Braswell, R. McKeown, D. S. Ojima, W. J. Parton, and W. Pulliam. 1996. Climate and nitrogen controls on the geography and timescales of terrestrial biogeochemical cycling. Global Biogeochemical Cycles **10**: 677–692.

Sellers, P. J. 1992. Biophysical models of land processes. Pages 451–490 *in* K. E. Trenberth, editor. Climate system modeling. Cambridge University Press, Cambridge, UK.

Sellers, P. J., Y. Mintz, Y. C. Sud, and A. Dalcher. 1986. A simple biosphere model (SiB) for use with general circulation models. Journal of the Atmospheric Sciences **43**(6): 505–531.

Sellers, P. J., et al. 1995. An overview of the ISLSCP Initiative I global data sets. *In* B. W. Meeson, F. E. Corprew, J. M. P. McManus, D. M. Myers, J. W. Closs, K. J. Sun, D. J. Sunday, and P. J. Sellers. ISLSCP Initiative I—global data sets for land–atmosphere models, 1987–1988. American Geophysical Union, Washington, D.C., USA. [Available on CD-ROM.]

Sellers, P. J., et al. 1997. Modeling the exchange of energy, water, and carbon between continents and the atmosphere. Science **275**:502–509.

Shinozaki, K., K. Yoda, K. Hozumi, and T. Kira. 1964*a*. A quantitative analysis of plant form—the pipe model theory. I. Basic analyses. Japanese Journal of Ecology **14**:97–105.

Shinozaki, K., K. Yoda, K. Hozumi, and T. Kira. 1964*b*. A quantitative analysis of plant form—the pipe model theory. II. Further evidence of the theory and its application in forest ecology. Japanese Journal of Ecology **14**:133–139.

Shugart, H. H. 1984. A theory of forest dynamics: the ecological implications of forest succession models. Springer-Verlag, New York, New York, USA.

Shugart, H. H., and S. W. Seagle. 1985. Modeling forest landscapes and the role of disturbance in ecosystems and communities. Pages 353–368 *in* S. T. A. Pickett and P. S. White, editors. The ecology of natural disturbance and patch dynamics. Academic Press, Orlando, Florida, USA.

Shugart, H. H., and T. M. Smith. 1996. A review of forest patch models and their application to global change research. Climate Change **34**:131–153.

Shugart, H. H., and D. C. West. 1977. Development of an Appalachian deciduous forest succession model and its application to assessment of the impact of the chestnut blight. Journal of Environmental Management **5**:161–179.

Smith, T. M., and M. A. Huston. 1989. A theory of the spatial and temporal dynamics of plant communities. Vegetatio **83**: 49–69.

Smith, T. M., R. Leemans, and H. Shugart. 1992. Sensitivity of terrestrial carbon storage to CO_2-induced climate change: comparison of four scenarios based on general circulation models. Climate Change **21**:367–384.

Smith, T. M., and D. L. Urban. 1988. Scale and resolution of forest structural pattern. Vegetatio **74**:143–150.

Solomon, A. M. 1986. Transient response of forests to CO_2-induced climate change: simulation modeling experiments in eastern North America. Oecologia **68**:567–579.

Swaine, M. D., D. Lieberman, and F. E. Putz. 1987. The dynamics of tree populations: a review. Journal of Tropical Ecology **3**:359–366.

Uhl, C. 1987. Factors controlling succession following slash-and-burn agriculture in Amazonia. Journal of Ecology **75**: 377–407.

Uhl, C., and C. F. Jordan. 1984. Succession and nutrient dynamics following forest cutting and burning in Amazonia. Ecology **65**:1476–1490.

Urban, D. L. 1990. A versatile model to simulate forest pattern: a user's guide to ZELIG version 1.0. Technical report. Environmental Sciences Department, University of Virginia, Charlottesville, Virginia, USA.

Van Wagner, C. E. 1977. Conditions for the start and spread of crown fire. Canadian Journal of Forest Research **7**:23–73.

VEMAP Members. 1995. Vegetation/ecosystem modeling and analysis project: comparing biogeography and biogeochemistry models in a continental-scale study of terrestrial ecosystem responses to climate change and CO_2 doubling. Global Biogeochemical Cycles **9**:407–434.

von Foerster, H. 1959. Some remarks on changing populations. Pages 328–407 *in* F. Stohlman, Jr., editor. Grune and Stratton, New York, New York, USA.

APPENDIX A

The detailed specification of leaf-level fluxes of carbon and water in the ecosystem demography (ED) model is available in ESA's Electronic Data Archive: *Ecological Archives* M071-008-A1.

APPENDIX B

The detailed specification of belowground limitation of leaf physiology in the ED model is available in ESA's Electronic Data Archive: *Ecological Archives* M071-008-A2.

APPENDIX C

The detailed specification of plant functional diversity in the ED model is available in ESA's Electronic Data Archive: *Ecological Archives* M071-008-A3.

APPENDIX D

The detailed specification of allocation and allometry in the ED model is available in ESA's Electronic Data Archive: *Ecological Archives* M071-008-A4.

APPENDIX E

The detailed specification of growth and reproduction in the ED model is available in ESA's Electronic Data Archive: *Ecological Archives* M071-008-A5.

APPENDIX F

The detailed specification of mortality in the ED model is available in ESA's Electronic Data Archive: *Ecological Archives* M071-008-A6.

APPENDIX G

The detailed specification of soil hydrology in the ED model is available in ESA's Electronic Data Archive: *Ecological Archives* M071-008-A7.

APPENDIX H

The detailed specification of organic-matter decomposition and nitrogen cycling in the ED model is available in ESA's Electronic Data Archive: *Ecological Archives* M071-008-A8.

APPENDIX I

The detailed specification of fire in the ED model is available in ESA's Electronic Data Archive: *Ecological Archives* M071-008-A9.

SUPPLEMENT

Supplementary material containing the source code for the ED model is available in ESA's Electronic Data Archive: *Ecological Archives* M071-008-S1.